

**This is the author's manuscript draft version of the contribution published as:**

**Lian, S., Wu, L., Nikolausz, M., Lechtenfeld, O.J., Richnow, H.H. (2019):**

<sup>2</sup>H and <sup>13</sup>C isotope fractionation analysis of organophosphorus compounds for characterizing transformation reactions in biogas slurry: Potential for anaerobic treatment of contaminated biomass

*Water Res.* **163**, art. 114882

**The publisher's version is available at:**

<http://dx.doi.org/10.1016/j.watres.2019.114882>

1           **<sup>2</sup>H and <sup>13</sup>C isotope fractionation analysis of organophosphorus compounds for**  
2           **characterizing transformation reactions in biogas slurry: Potential for anaerobic**  
3           **treatment of contaminated biomass**  
4

5 Shujuan Lian<sup>1</sup>, Langping Wu<sup>1</sup>, Marcell Nikolausz<sup>2</sup>, Oliver J. Lechtenfeld<sup>3</sup>, Hans H. Richnow<sup>1\*</sup>

6 <sup>1</sup> Department of Isotope Biogeochemistry, Helmholtz Centre for Environmental Research-UFZ,  
7 Permoserstraße 15, 04318 Leipzig, Germany

8 <sup>2</sup> Department of Environmental Microbiology, Helmholtz Centre for Environmental Research-  
9 UFZ, Permoserstraße 15, 04318 Leipzig, Germany

10 <sup>3</sup>Department of Analytical Chemistry, Helmholtz Centre for Environmental Research-UFZ,  
11 Permoserstraße 15, 04318 Leipzig, Germany

12 shujuan.lian@ufz.de

13 langping.wu@ufz.de

14 marcell.nikolausz@ufz.de

15 oliver.lechtenfeld@ufz.de

16 \*Corresponding author. Tel.: +49 341 2351 212; fax: +49 341 451 212. E-mail address:

17 hans.richnow@ufz.de

18 **Abstract**

19 The ability of anaerobic digestion (AD) to eliminate organophosphorus model compounds (OPs)  
20 with structural elements of phosphate, phosphorothioate and phosphorodithioate esters was  
21 studied. The enzymatic mechanism of the first irreversible degradation reaction was  
22 characterized using metabolite pattern and kinetic  $^2\text{H}/^{13}\text{C}$ -isotope effect in original, cell-free and  
23 heat sterilized biogas slurry. The isotope fractionation study suggests different modes of  
24 degradation reactions. Representatives for phosphate ester, tris(2-chloroethyl) phosphate and  
25 tris(1,3-dichloro-2-propyl) phosphate, were hydrolyzed in biogas slurry without carbon or  
26 hydrogen isotope fractionation. Representatives for phosphorodithioate, Dimethoate and  
27 Malathion, were degraded in original slurry yielding carbon enrichment factor ( $\epsilon_C$ ) of  $-0.6 \pm 0.1\text{‰}$   
28 and  $-5.5 \pm 0.1\text{‰}$  ( $-0.9 \pm 0.1\text{‰}$  and  $-7.2 \pm 0.5\text{‰}$  in cell-free slurry), without hydrogen isotope  
29 fractionation. Phosphorothioate degradation represented by Parathion and Parathion-methyl  
30 yielded surprisingly different  $\epsilon_C$  ( $-0.7 \pm 0.2$  and  $-3.6 \pm 0.4\text{‰}$ ) and  $\epsilon_H$  ( $-33 \pm 5$  and  $-5 \pm 1\text{‰}$ ) in  
31 original slurry compared to cell-free slurry ( $\epsilon_C = -2.5 \pm 0.5$  and  $-8.6 \pm 1.4\text{‰}$ ;  $\epsilon_H = -61 \pm 10$  and -  
32  $10 \pm 3\text{‰}$ ) suggesting H-C bond cleavage. Degradation of Parathion and Parathion-methyl in  
33 sterilized slurry gave carbon but not hydrogen fractionation implying relative thermostable  
34 enzymatic activity with different mechanism. The correlation of  $^2\text{H}$  and  $^{13}\text{C}$  stable isotope  
35 fractionation of Parathion in biogas slurry showed distinct pattern ( $\Lambda_{\text{original}} = 31 \pm 11$ ,  $\Lambda_{\text{cell-free}} =$   
36  $20 \pm 2$ ), indicating different mechanism from chemical hydrolysis. Overall, AD can be a  
37 potential treatment for OPs contaminated biomass or contaminated organic waste material.

38 **Key words:** Organophosphorus compounds, enzymatic hydrolysis, biogas reactor, two  
39 dimensional compound-specific stable isotope analysis, isotope fractionation, reaction  
40 mechanism

## 41        **1. Introduction**

42 Synthetic organophosphorus compounds (OPs) have been produced for various purposes. Most  
43 of them are used as pesticides, plasticizers, air fuel ingredients and chemical warfare agents  
44 (Singh and Walker, 2006). OPs constitute the largest group of insecticides, accounting for an  
45 estimated 34% of world-wide sales, compared with other types of insecticides, such as carbamate  
46 and organochlorine compounds (Chanda et al., 2006; Karami-Mohajeri and Abdollahi, 2010).  
47 Biomass may be contaminated with residual OP pesticides (Battersby and Wilson, 1989; Kupper  
48 et al., 2008), and the waste material from crops or organic wastes containing OPs (Pang et al.,  
49 2018) could be well used for biogas production. The efficiency and robustness of degradation  
50 need to be assessed for the development of biotechnological strategies on treating organic waste  
51 in biogas producing anaerobic digestion (AD) systems.

52 Thus, the monitoring and characterization of OPs degradation in AD system is an important  
53 aspect for developing treatment concepts. Knowledge on degradation mechanisms might be used  
54 to optimize the reduction of residual concentration in digestate. Till now, degradation of OPs has  
55 been investigated in natural water systems (Druzina and Stegu, 2007), soils (Singh et al., 2005),  
56 sediments (Graetz et al., 1970) and bioreactors (Li et al., 2008). The fates of OPs in environment  
57 comprise both biotic transformation via microorganisms and abiotic processes. The hydrolysis is  
58 assumed as the most important step for detoxification of OPs (Singh and Walker, 2006; Theriot  
59 and Grunden, 2011). The biotic and chemical hydrolysis of OPs proceeds probably  
60 simultaneously in AD.

61 OPs contain three main core structures based on the oxygen or sulfur atom position: phosphate,  
62 phosphorothioate and phosphorodithioate (Sogorb and Vilanova, 2002). In this study, six typical

63 OPs (tris(2-chloroethyl) phosphate (TCEP), tris(1,3-dichloro-2-propyl) phosphate (TDCPP),  
64 Parathion, Parathion-methyl, Dimethoate and Malathion) were chosen as model compounds to  
65 investigate transformation containing phosphate, phosphorothioate and phosphorodithioate in  
66 AD system. TCEP and TDCPP appear to be the most recalcitrant and are ubiquitous flame  
67 retardants in the environment (Ding et al., 2015; Reemtsma et al., 2008). Degradations of  
68 Parathion and Parathion-methyl were observed in anoxic soils via reduction and hydrolysis  
69 (Adhya et al., 1981). Several researchers reported the reductive transformation of Parathion and  
70 Parathion-methyl by anaerobic microorganisms (Barton et al., 2004; Guo and Jans, 2006; Katan  
71 et al., 1976; Yang et al., 2007). A long adaption time was needed to reach the complete removal  
72 of Dimethoate in an expanded granular sludge bed reactor (Monsalvo et al., 2014). A  
73 Dimethoate-degrading enzyme from *Aspergillus niger* ZHY256 isolated from sewage and the  
74 soil of highly contaminated cotton field was reported (Liu et al., 2001). Biodegradation of  
75 Malathion was found in estuarine waters (Lacorte et al., 1995), as well as with *Acinetobacter*  
76 strain *baumannii* AFA isolated from domestic sewage in Egypt (Azmy et al., 2015). Hydrolysis  
77 was found to be an important biodegradation pathway of OPs under aerobic and anaerobic  
78 conditions (Singh, 2009; Singh and Walker, 2006; Theriot and Grunden, 2011).

79 To improve degradation rate and promote investigation on the fate of OPs, the identification of  
80 degradation mechanism in AD is crucial. Multi-element fingerprinting of chemicals via  
81 compound-specific stable isotope analysis (CSIA) was applied to trace the degradation  
82 mechanisms making use of isotope fractionation concepts (Meyer et al., 2009; Penning et al.,  
83 2010; Zhang et al., 2015). Several studies on CSIA to trace abiotic hydrolysis of OPs have been  
84 reported (Wu et al., 2018a, 2017, 2014). A recent study on natural attenuation of Parathion by

85 hydrolysis at a contaminated field site in Denmark using CSIA was described (Wu et al., 2018b),  
86 indicating that the isotope fractionation pattern has potential to characterize and monitor  
87 hydrolysis in field studies. Moreover, application of CSIA for investigating the  
88 biotransformation of hexachlorocyclohexanes in biogas slurry has been recently published (Lian  
89 et al., 2018). To our best knowledge this is the first report that elucidates biotransformation of  
90 OPs in biogas reactors making use of isotope fractionation to characterize the bond cleavage of  
91 the initial degradation reactions steps.

92 This study intends to evaluate the degradation mechanism of phosphate, phosphorothioate and  
93 phosphorodithioate derivatives in AD, using biogas slurries from a pilot-scale biogas plant as a  
94 model system. In case of effective transformation, phytoremediation (Peuke and Rennenberg,  
95 2005) combined with AD can also be considered as a potential strategy for environmental  
96 cleanup (Lian et al., 2018). The specific objectives of this study were to: (i) assess  
97 biodegradation of OPs in the original biogas slurry in order to evaluate the capability of microbes  
98 for OPs elimination; (ii) monitor enzymatic hydrolytic activity in cell-free slurry (slurry after  
99 centrifugation and filtration with a 0.22  $\mu\text{m}$  filter to remove cells) and identify the similarity of  
100 degradation mechanism in original slurry; (iii) characterize the degradation pathways of OPs by  
101 dual C-H isotope fractionation patterns. The potential of biogas reactors to degrade OPs could be  
102 exploited to treat contaminated waste materials and CSIA could be useful for characterizing and  
103 monitoring the degradation pathways.

## 104 **2. Materials and Methods**

## 105        **2.1 Chemicals**

106    TCEP (tris(2-chloroethyl) phosphate, analytical standard, 97.0% pure), TDCPP (tris(1,3-  
107    dichloro-2-propyl) phosphate, 95.7% pure), Parathion (*O,O*-diethyl-*O*-(4-nitrophenyl)  
108    phosphorothioate, analytical standard, 99.7% pure), Parathion-methyl (*O,O*-dimethyl-*O*-(4-  
109    nitrophenyl) phosphorothioate, analytical standard, 99.8% pure), Dimethoate (*O,O*-dimethyl *S*-  
110    [2-(methylamino)-2-oxoethyl] phosphorodithioate, analytical standard, 99.6% pure), Malathion  
111    (*O,O*-dimethyl *S*-(1,2-dicarbethoxyethyl) phosphorodithioate, analytical standard, 99.7% pure),  
112    Dichlorvos (2,2-dichlorovinyl dimethyl phosphate, analytical standard, 98.8% pure) and tris base  
113    (2-Amino-2-(hydroxymethyl)-1,3-propanediol) were obtained from Sigma-Aldrich (Munich,  
114    Germany). Anhydrous Na<sub>2</sub>SO<sub>4</sub> (extra pure) and hydrochloric acid (HCl) were purchased from  
115    Merck (Darmstadt, Germany).

## 116        **2.2 Anaerobic biogas slurry**

117    Biogas slurry (total solids (TS) = 6.84%, volatile solids = 77.34% of TS) was taken from a pilot-  
118    scale biogas plant operated with an organic loading rate of 3.5 g<sub>vs</sub>L<sup>-1</sup>day<sup>-1</sup> and hydraulic retention  
119    time of 47 days, utilizing maize silage and cattle manure as main substrates. The slurry was  
120    sieved (1cm) before using for biodegradation assays.

## 121        **2.3 OPs biodegradation assays with biogas slurry**

122    For assessing biodegradation of OPs in AD system, the original slurry was used. The cell-free  
123    supernatant was assigned for study on enzymatic hydrolysis of OPs. In order to obtain the cell-  
124    free fraction, slurry from biogas reactor was centrifuged at 16,100 × g (4 °C) for 20 min to

125 remove solid particles, and then the supernatant was filtered through a 0.22  $\mu\text{m}$  membrane filter  
126 (Merck Millipore). The slurry was autoclaved (121  $^{\circ}\text{C}$ , 30 min) three times in bottles for  
127 sterilized control experiments.

128 Thus, four sets of experiments were conducted simultaneously: (i) original slurry directly taken  
129 from the biogas plant was used to detect the capability of microbes for OPs degradation; (ii) cell-  
130 free slurry after centrifugation and filtration (see above) was utilized to analyze the hydrolytic  
131 activity of extracellular enzymes; (iii) sterilized slurry was used for assuming that cells were  
132 killed and enzyme activity were inactivated by elevated temperature typical for sterilization; (iv)  
133 chemical hydrolysis experiments of OP with tris-HCl buffer at pH 7.4 was conducted as an  
134 abiotic control.

135 Original slurry was initially tested to transform Parathion and Parathion-methyl initially, but the  
136 reaction was too rapid to analyze the associated isotope fractionation. Therefore, a 50-fold  
137 dilution of original slurry was used after a series of dilution experiments, in order to reduce the  
138 rate of reaction for obtaining first order rate constants and fractionation factors. For the original  
139 slurry assays and cell-free slurry assays of Parathion and Parathion-methyl, 1 mL original slurry  
140 or 1 mL cell-free supernatant were directly added into the prepared bottles and diluted. For  
141 TCEP and TDCPP degradation experiment slurry after 25-fold dilution was taken. The  
142 degradation rates of Dimethoate and Malathion were obtained after 5-fold dilution. The cell-free  
143 and sterilized slurry were conducted with the same dilution as the original slurry experiments for  
144 all tested OPs.

145 All experiments were performed at 37 °C, in 120 mL serum bottles containing 50 mL of 10 mM  
146 tris-HCl buffer and adjusted to pH 7.4 with 6 N HCl. The bottles with 70 mL headspace were  
147 flushed with N<sub>2</sub>/CO<sub>2</sub> (80%/20%, v/v) for at least 15 min to maintain anoxic condition and  
148 crimped with Teflon™-coated butyl rubber septa. Afterwards, the corresponding slurries were  
149 added into bottles in the anaerobic box according to different fold dilutions for each OP. The  
150 mixtures were incubated at 37 °C for 1 hour before adding the stock solutions of OPs. Stock  
151 solutions of OPs dissolved in acetone were added into serum bottles respectively to achieve the  
152 intended initial concentrations as described in **Supporting Information (SI) section S1, Table**  
153 **S1**.

#### 154 **2.4 Extraction**

155 Parallel batch bottles were sacrificed at different time intervals for each OP compound. The  
156 reactions were stopped with 6 N HCl to inactivate the enzymes by adjusting pH to 5 for  
157 Parathion and Parathion-methyl assays to avoid further hydrolysis at acid condition and below  
158 pH 4 for other experiments. Control experiments were treated identically. Subsequently, 2 mL of  
159 dichloromethane (DCM) containing Dichlorvos as an internal standard was added to extract  
160 residual OPs and the metabolites. All bottles were shaken at 180 rpm for 2 hours and the organic  
161 phase with DCM was separated and transferred into screwed vials with a glass syringe. For  
162 cleanup of organic phase, the method was the same as previous study (Lian et al., 2018) but elute  
163 solvent was DCM (see **Section S2.2** in **SI**). Extracts were stored at -20 °C until further analysis.

164        **2.5 Analytical methods**

165        **2.5.1 Concentration**

166    An Agilent 6890 series gas chromatograph (GC) (Agilent Technologies, Germany) equipped  
167    with a flame ionization detector (FID) was used to determine the concentration. OPs were  
168    separated using a HP-5 column (30 m length \* 320  $\mu\text{m}$  inner diameter \* 0.25  $\mu\text{m}$  thickness,  
169    Agilent, USA) with 1.5 mL  $\text{min}^{-1}$  helium flow as the carrier gas. The temperature program was:  
170    60  $^{\circ}\text{C}$  for 2 min, increased by 10  $^{\circ}\text{C min}^{-1}$  to 160  $^{\circ}\text{C}$ , followed by 5  $^{\circ}\text{C min}^{-1}$  to 220  $^{\circ}\text{C}$  and by 15  $^{\circ}\text{C}$   
171     $\text{min}^{-1}$  to 280  $^{\circ}\text{C}$ , and held for 2 min isotherm (Wu et al., 2018a). The temperatures of injector and  
172    detector were set to 180  $^{\circ}\text{C}$  and 280  $^{\circ}\text{C}$ , respectively.

173        **2.5.2 Isotope composition**

174    The carbon isotope composition was analyzed by an isotope ratio mass spectrometry (IRMS)  
175    system (Finnigan MAT 252, Thermo Fischer Scientific) consisting of a GC (Agilent 6890)  
176    coupled with a GC/C III interface to IRMS (Wu et al., 2017). For analysis of hydrogen isotope  
177    composition, the samples were analyzed with GC–chromium-based high-temperature  
178    conversion–IRMS system (Renpenning et al., 2015; Wu et al., 2017). Thermal decomposition of  
179    OPs in GC injector may cause isotope fractionation, thus, the deactivation of glass liner using  
180    BSTFA (*N,O*-bis (trimethylsilyl) trifluoroacetamide) was needed. Detailed information of  
181    deactivation is given in **SI, section S2**.

182    Isotope compositions are reported with notation  $\delta$  (**Eq. 1**) in parts per thousand.  $R_{\text{sample}}$  is the  
183    ratio of  $^{13}\text{C}/^{12}\text{C}$  (or D/H) in the sample, and  $R_{\text{standard}}$  is the ratio based on the international isotope  
184    standard: Vienna Pee Dee Belemnite (V-PDB) for carbon and Vienna Standard Mean Ocean

185 Water (V-SMOW) for hydrogen, respectively (Coplen et al., 2006; Gehre et al., 2015).

$$186 \quad \delta = \frac{R_{\text{sample}} - R_{\text{standard}}}{R_{\text{standard}}} \quad (1)$$

187 Isotope enrichment factor ( $\epsilon$ ) is determined with the logarithmic form of the Rayleigh equation

188 (**Eq. 2**) for quantification of the isotope fractionation (Mariotti et al., 1981; Rayleigh, 1896).

189 Notations  $\delta_t$  and  $\delta_0$  are the isotopic compositions ( $C_t$  and  $C_0$  are the concentrations) of the

190 substrate at time  $t$  and time  $0$ , respectively.

$$191 \quad \ln\left(\frac{\delta_t+1}{\delta_0+1}\right) = \epsilon * \ln\left(\frac{C_t}{C_0}\right) \quad (2)$$

192 The relationship between carbon and hydrogen fractionation ( $\Lambda$ ) is described by the slope of

193 linear regression between  $\Delta\delta^2\text{H}$  and  $\Delta\delta^{13}\text{C}$  (**Eq. 3**). To correct the variation, shifts for hydrogen

194 ( $\Delta\delta^2\text{H}$ ) and carbon ( $\Delta\delta^{13}\text{C}$ ) are calculated by subtracting the isotopic signature at time  $t$  from the

195 initial value ( $\Delta\delta = \delta_0 - \delta_t$ ). An approximation of  $\Lambda$  is the correlation of  $\epsilon_H$  and  $\epsilon_C$ .

$$196 \quad \Lambda = \frac{\Delta\delta^{2\text{H}}}{\Delta\delta^{13\text{C}}} \approx \frac{\epsilon_H}{\epsilon_C} \quad (3)$$

### 197 **2.5.3 Identification of metabolites**

198 The GC amenable products in DCM extracts were analyzed via a GC (7890A, Agilent

199 Technologies, Palo, USA)-mass spectrometry (MS) (5975C, Agilent Technologies, Palo, USA).

200 Since some of the OPs metabolites in biogas slurry were hydrophilic and not GC amenable, they

201 were characterized via an ultra-high resolution Fourier-transform ion cyclotron resonance (FT-

202 ICR)-MS using a Solarix XR 12 T (Bruker Daltonics, Germany) and UPLC-Q-Tof-MSA

203 (Waters, USA). Samples with ca. 50% degradation of OPs were selected and 10 mL of aqueous  
204 solution centrifuged at  $16,100 \times g$  ( $4 \text{ }^\circ\text{C}$ ) for 20 min was extracted by solid phase extraction (SPE)  
205 with 100 mg Bond Elut PPL cartridges (Agilent Technologies, USA) for analysis of metabolites.  
206 Detailed information is described in **SI, section S5.1**.

### 207 **3. Results**

208 During biotransformation of the six typical OPs in biogas slurry, the first irreversible degradation  
209 step was deduced based on metabolite analysis (**Scheme 1** and **Scheme S2, SI**) and isotope  
210 fractionation. The degradation curves could be described by the first order reaction (**Fig. 2** and  
211 **Fig. S2, SI**), suggesting that Rayleigh concept can be used to quantify the  $^2\text{H}$  and  $^{13}\text{C}$  isotope  
212 fractionations. The isotope fractionation pattern provides further evidence for the first bond  
213 cleavage reaction for the interpretation of OPs transformation pathway.

#### 214 **3.1 Degradation of phosphate esters in biogas slurry**

215 TCEP and TDCPP were studied as representatives of phosphate esters. The degradation with  
216 original slurry after 25-fold dilution was conducted for acquiring the isotope fractionation. TCEP  
217 and TDCPP were transformed to ca. 70% with rate constants ( $\times 10^{-3} \text{ h}^{-1}$ ) of  $3.1 \pm 0.5$  and  $2.6 \pm$   
218  $0.4$  in original slurry compared to lower rates of  $0.8 \pm 0.1$  and  $2.4 \pm 0.3$  in cell-free slurry,  
219 respectively. Bis(2-chloroethyl) hydrogen phosphate was tentatively identified in the degradation  
220 experiment of TCEP and bis(1,3-dichloro-2-propanyl) hydrogen phosphate in the degradation  
221 experiment of TDCPP suggesting that hydrolysis lead to cleavage of the phosphate ester bond  
222 (**Table S2** and **S3, SI**).

223 Constant concentrations were found indicating no significant degradation of phosphate esters in  
224 the sterilized slurry (**Fig. S1, SI**). Neither carbon nor hydrogen isotope enrichment was observed  
225 (**Table 1**) suggesting that probably no H or C bond cleavage was involved in the first irreversible  
226 reaction step and hydrolysis is the dominant reaction. Hydrolysis reactions were found in  
227 experiments with phosphate esters and liver microsomes as a side reaction which can occur also  
228 spontaneously also without activation (Van den Eede et al., 2013). Combining the information  
229 from detected products in experiments of both phosphate esters and the absence of carbon  
230 isotope fractionation, hydrolysis of P-O bond was assumed to be the first irreversible step.

### 231 **3.2 Degradation of phosphorothioate in biogas slurry**

232 Parathion and parathion-methyl selected as representatives for phosphorothioate were  
233 transformed rapidly in the biogas slurry. Thus, 50-fold dilution was used to slow down reaction  
234 in the original slurry for achieving stable isotope fractionation and it gave rate constants ( $\times 10^{-3}$   
235  $\text{h}^{-1}$ ) of  $12.8 \pm 1.2$  and  $10.5 \pm 1.0$ , respectively. The degradation of Parathion and Parathion-  
236 methyl with the cell-free slurry was slower and could be described by rate constants ( $\times 10^{-3} \text{h}^{-1}$ )  
237 of  $2.8 \pm 0.3$  and  $5.3 \pm 0.5$ , respectively. The degradation in 50-fold diluted sterilized slurry gave  
238 rate constants ( $\times 10^{-3} \text{h}^{-1}$ ) of  $2.1 \pm 0.2$  and  $3.5 \pm 0.3$  for Parathion and Parathion-methyl  
239 respectively showing that enzymatic activity was preserved after heat treatment.

240 Amino-parathion and amino-parathion-methyl were detected in biogas slurry degradation  
241 experiments both via GC-MS (**Fig. S4-S5, SI**) and FT-ICR MS analysis (**Table S4-S5, Fig. S8**  
242 and **S15-S16, SI**), indicating reduction of the nitro group. *O*-ethyl *O*-(4-nitrophenyl)  
243 phosphorothioate and p-nitrophenol were detected in negative mode by FT-ICR MS and

244 confirmed via LCMS, implying hydrolysis of Parathion. *O*-ethyl *O*-(4-aminophenyl)-  
245 phosphorothioate was observed in biogas slurry experiments (**Fig. S9-S11, SI**), implying  
246 reduction of the nitro group of parathion. Tentatively, *O*-ethyl *O*-(1,1-ethanediyl) *O*-(4-  
247 nitrophenyl) phosphorothioate and *O*-ethyl *O*-(1,1-ethanediyl) *O*-(4-aminophenyl)  
248 phosphorothioate were found (**Table S4 and Fig. S12-S13, SI**), suggesting a hydroxylation of the  
249 side chain. The detection of *O*-methyl *O*-(4-nitrophenyl) phosphorothioate (**Fig. S14, SI**) and p-  
250 nitrophenol with increasing intensity over time in the degradation experiments with Parathion-  
251 methyl suggests hydrolysis reaction.

252 The  $\delta^{13}\text{C}$  values of Parathion-methyl were enriched from  $-32.9 \pm 0.3\text{‰}$  to  $-28.5 \pm 0.4\text{‰}$  with  $\epsilon_{\text{C}}$   
253 of  $-3.6 \pm 0.4\text{‰}$  in original slurry experiment upon about 75% degradation. Carbon isotope  
254 enrichment from  $-31.4 \pm 0.1\text{‰}$  to  $-18.6 \pm 0.5\text{‰}$  with  $\epsilon_{\text{C}}$  of  $-8.6 \pm 1.4\text{‰}$  was found in experiments  
255 with cell-free supernatant after 80% transformation. Accordingly, the  $\delta^2\text{H}$  isotope composition of  
256 Parathion-methyl in original slurry changed from  $-126.4 \pm 0.5\text{‰}$  to  $-111.1 \pm 1.6\text{‰}$  and yielded a  
257  $\epsilon_{\text{H}}$  of  $-5 \pm 1\text{‰}$ . In the experiment with cell-free supernatant the  $^2\text{H}$  isotope composition of  
258 Parathion-methyl shifted from  $-122.5 \pm 1.4\text{‰}$  to  $-115.1 \pm 3.7\text{‰}$  and yielded a  $\epsilon_{\text{H}}$  of  $-10 \pm 3\text{‰}$   
259 (**Fig. 1 and Fig. 3**).

260 During biodegradation of Parathion slight carbon enrichment was discovered with a change from  
261  $-27.0 \pm 0.2\text{‰}$  to  $-25.6 \pm 0.4\text{‰}$ , yielding a  $\epsilon_{\text{C}}$  of  $-0.7 \pm 0.2\text{‰}$  in original slurry. Similarly, the  $\delta^{13}\text{C}$   
262 values shifted from  $-29.2 \pm 0.4\text{‰}$  to  $-26.7 \pm 0.6\text{‰}$  and resulted in a  $\epsilon_{\text{C}}$  of  $-2.5 \pm 0.5\text{‰}$  in cell-free  
263 slurry upon 80% degradation. A strong  $^2\text{H}$  enrichment in original slurry from  $-139.1 \pm 2.1\text{‰}$  to -  
264  $92.5 \pm 5.6\text{‰}$  gave a  $\epsilon_{\text{H}}$  of  $-33 \pm 5\text{‰}$ . In the cell-free supernatant an enrichment from  $-132.1 \pm 2.8\text{‰}$

265 to  $-84.4 \pm 3.8\text{‰}$  with a  $\epsilon_{\text{H}}$  of  $-61 \pm 10\text{‰}$  during the biodegradation of Parathion was observed  
266 (**Fig. 1** and **Fig.3**).

### 267 **3.3 Degradation of phosphorodithioates in biogas slurry**

268 Dimethoate and Malathion as the representatives for phosphorodithioates were rapidly degraded  
269 in the slurry and a 5-fold dilution was selected for isotope fractionation experiments to slow  
270 down the reaction. With this dilution Dimethoate and Malathion were transformed up to around  
271 80% after 40 hours with rate constants ( $\times 10^{-3} \text{ h}^{-1}$ ) of  $39.6 \pm 7.9$  and  $50.5 \pm 5.3$  in original slurry  
272 ( $33.3 \pm 5.5$  and  $35.5 \pm 6.7$  in the cell-free slurry), respectively. The degradation rate constant of  
273 Dimethoate in the sterilized slurry was  $14.8 \pm 3.5 \times 10^{-3} \text{ h}^{-1}$  (**Fig. S2, SI**). No degradation of  
274 Malathion was detected in sterilized slurry (**Fig. S1, SI**).

275 In experiment with Dimethoate, *O,O,S*-trimethyl phosphorodithioate was detected by GC-MS  
276 (**Fig. S6, SI**). *O,O*-dimethyl S-[2-(methylamino)-2-oxoethyl] dithiophosphate, *O,O*-dimethyl  
277 hydrogen phosphorodithioate and *O,O*-dimethyl hydrogen phosphorothioate were observed by  
278 FT-ICR MS (**Table S6, SI**). In the experiments with Malathion, diethyl succinate and diethyl  
279 (2E)-2-butenedioate were found using GC-MS (**Fig. S7, SI**). The FT-ICR MS detected exact  
280 masses corresponding to diethyl 2-[[hydroxy(methoxy)phosphorothioyl]sulfanyl]succinate,  
281 *O,O*-dimethyl hydrogen phosphorodithioate and *O,O*-dimethyl hydrogen phosphorothioate as  
282 metabolites (**Table S7, SI**).

283 The  $\delta^{13}\text{C}$  of Dimethoate slightly enriched from  $-39.1 \pm 0.3\text{‰}$  to  $-37.4 \pm 0.2\text{‰}$  and yielded a  $\epsilon_{\text{C}}$  of  
284  $-0.6 \pm 0.1\text{‰}$  upon 79% degradation in original slurry. Enrichment from  $-39.2 \pm 0.1\text{‰}$  to  $-37.2 \pm$   
285  $0.1\text{‰}$  upon 75% degradation was detected in cell-free slurry, yielding a  $\epsilon_{\text{C}}$  of  $-0.9 \pm 0.1 \text{‰}$  (**Fig.**

286 **S1 and S3, SI**). The carbon isotope fractionation indicated that a carbon bond cleavage was  
287 involved in the first irreversible rate limiting reaction step. No  $^2\text{H}$  fractionation could be detected  
288 suggesting that no H bond cleavage was involved.

289 The  $\delta^{13}\text{C}$  values of Malathion were enriched from  $-26.5 \pm 0.5\text{‰}$  to  $-14.9 \pm 0.4\text{‰}$  after 88%  
290 transformation in the original slurry and from  $-25.7 \pm 0.5\text{‰}$  to  $-15.2 \pm 0.4\text{‰}$  after 77%  
291 degradation in the cell-free slurry, resulting in  $\epsilon_{\text{C}}$  values of  $-5.5 \pm 0.1\text{‰}$  and  $-7.2 \pm 0.5 \text{‰}$ ,  
292 respectively (**Fig. S1 and S3, SI**). The transformation of Malathion in biogas slurry was not  
293 associated with detectable hydrogen isotope fractionation. Similar to phosphate esters, Malathion  
294 did not degrade in sterilized slurry.

## 295 **4. Discussion**

### 296 **4.1 Interpretation of transformation mechanisms**

297 The transformation of OPs is suggested to be predominated by biodegradation compared to  
298 abiotic degradation processes in natural environment (Zhang and Bennett, 2005). In this study,  
299 biodegradation of OPs was governed by hydrolysis and reduction reactions, as predicted in  
300 anaerobic aquatic system (Druzina and Stegu, 2007). The anaerobic digestion reactor showed a  
301 high potential for hydrolytic reactions and the hydrolysis was remarkably faster than expected  
302 for chemical hydrolysis. We intended to study the structure-activity relationship on degradation  
303 of OPs in AD at neutral condition, the half-life times of OPs in AD system decreased in the order  
304 of original slurry < cell-free slurry < sterilized slurry (**Fig. 2 and Fig. S2, SI**). The results  
305 showed a high capability for hydrolysis in cell-free slurry via exoenzymes which may be

306 abundant in the AD reactor. Hydrolases are key enzymes in the AD system (Gasch et al., 2013)  
307 and our results showed that they can degrade OPs.

#### 308 **4.1.1 Degradation of phosphate esters**

309 No  $^2\text{H}$  and  $^{13}\text{C}$  isotope fractionation of phosphate esters was found, similar to alkaline hydrolysis.  
310 This suggested that hydrolysis at P-O bond was the rate limiting reaction step, which was  
311 consistent with the detection of metabolites. The isotope fractionation indicated an enzymatic  
312 hydrolysis with P-O bond cleavage in biogas slurry probably by an esterase using an  $\text{S}_{\text{N}}2$   
313 mechanism (**Scheme S2, SI**). The potential to monitor hydrolysis of phosphate esters employing  
314  $^2\text{H}$  and  $^{13}\text{C}$  isotope fractionation was low as neither C nor H bond was cleaved. The advantage of  
315 isotope fingerprint is that it can give hint on the reaction deduction via enrichment factor when  
316 the intermediate is not easy to determine or is further degraded.

#### 317 **4.1.2 Degradation of phosphorothioates**

318 The transformation kinetic of both phosphorothioates decreased in the experiment with living  
319 cells, enzyme extracts and heat treated autoclaved slurry showing a robust capability for  
320 degradation. The proposed transformation mechanisms for Parathion and Parathion-methyl are  
321 summarized below (see **Scheme 1**): (i) biotic hydrolysis via esterase caused by P-O cleavage  
322 (Wanamaker et al., 2013), which is not expected to lead to isotope fractionation of  $^2\text{H}$  and  $^{13}\text{C}$ .  
323 Thus, the contribution of this reaction could not be directly evaluated via isotope fractionation;  
324 (ii) the hydrolysis of a C-O bond cleaving the alkyl side chain via  $\text{S}_{\text{N}}2$  reaction, leading to  $^{13}\text{C}$   
325 fractionation and no  $^2\text{H}$  fractionation (Wanamaker et al., 2013; Wu et al., 2018a); (iii) the  
326 reduction reaction of  $\text{NO}_2$  to  $\text{NH}_2$ , which will not lead to  $^2\text{H}$  or  $^{13}\text{C}$  fractionation but took place

327 as we observed the reduction of the nitro group; (iv) the dehydrogenation leading to C-H  
328 cleavage at the side chain of parathion which infers a radical reaction in the rate limiting reaction  
329 step likely caused by dehydrogenase. The pronounced  $^2\text{H}$  and low  $^{13}\text{C}$  isotope fractionation in the  
330 experiments of original slurry and cell-free slurry suggested this dominant reaction other than  
331 hydrolysis (**Table 1**). The contribution of dehydrogenation reaction was lower taking the  
332 fractionation pattern of Parathion-methyl into account, showing larger  $^{13}\text{C}$  ( $\epsilon_{\text{C}} = -8.6 \pm 1.4$ ) and  
333 lower  $^2\text{H}$  ( $\epsilon_{\text{H}} = -10 \pm 3$ ) isotope fractionation compared to Parathion. The extent of  $^{13}\text{C}$  isotope  
334 fractionation may suggest that hydrolysis reaction with C-O bond cleavage was the rate limiting  
335 step for parathion-methyl. In summary, parallel reactions can catalyze the transformation of  
336 phosphorothioates in AD systems showing a functional redundancy and implying a robust  
337 capability to transform and possibly detoxify phosphorothioates.

### 338 **4.1.3 Degradation of phosphorodithioates**

339 The degradation kinetic of Dimethoate showed a similar pattern as phosphorothioates with  
340 decreasing rate constants comparing original slurry, cell free slurry and heat treated autoclaved  
341 slurry. The latter still showed a robust capability for degradation. In contrast, the heat treated  
342 autoclaved slurry lost capability to degrade Malathion. The metabolites of Dimethoate and  
343 Malathion in AD system gave the hint on: (i) hydrolysis with C-O cleavage (**Scheme S2, SI**); (ii)  
344 hydrolysis with C-S cleavage; (iii) enzymatic hydrolysis leading to P-S cleavage of  
345 phosphorodithioate. The detected carbon isotope effect was consistent with metabolites formed  
346 by C-O or C-S bond cleavage in the rate limiting reaction step. The carbon isotope effect of  
347 Dimethoate was much smaller compared to Malathion implying that the contribution of a C bond  
348 cleavage was higher in the original and cell-free slurry experiment with Malathion. The

349 hydrolysis mechanism of phosphorodithioates in AD was distinguished from neutral chemical  
350 hydrolysis as indicated by the different extent of isotope fractionation. The P-S bond cleavage is  
351 not expected to yield a primary  $^2\text{H}$  or  $^{13}\text{C}$  KIE isotope effect and the contribution of these types  
352 of bond cleavage could not be evaluated in this work.

## 353 **4.2 Diagnostic potential of two-dimensional isotope fractionation**

### 354 **4.2.1 Carbon isotope fractionation**

355 For degradation of phosphorothioate in biogas slurry, an increase in  $\epsilon_{\text{C}}$  values for both  
356 compounds was obtained from original slurry to cell-free slurry and sterilized slurry (**Table 1**),  
357 suggesting different contribution of the particular reactions. The  $^{13}\text{C}$  isotope fractionation was  
358 probably dominated by C-O bond cleavage and the slightly depleted carbon isotope fractionation  
359 could be assumed due to the contribution of P-O cleavage by phosphotriesterases (PTE) or  
360 reduction of the nitrogen group (Munnecke, 1976; Serdar and Gibson, 1985). The  $\epsilon_{\text{C}}$  value in  
361 sterilized slurry with parathion-methyl ( $-10.3 \pm 0.1$ ) was close to chemical neutral hydrolysis at  
362 pH 7 ( $-9.9 \pm 0.7\text{‰}$ ), indicating a dominant mechanism of C-O bond cleavage. The  $\epsilon_{\text{C}}$  of  
363 Parathion in sterilized slurry (pH 7.4,  $-4.3 \pm 0.4\text{‰}$ ) was lower than chemical hydrolysis under  
364 neutral conditions at pH 7 ( $-6.0 \pm 0.2\text{‰}$ ) (Wu et al., 2018a), implying distinct mechanism of the  
365 relative thermostable enzymatic activity (Brock, 1985).

366 The same phenomenon was observed for phosphorodithioates, an increase in  $\epsilon_{\text{C}}$  values for both  
367 compounds was obtained from original slurry to cell-free slurry and sterilized slurry (**Table 1**),  
368 with more contribution of P-S cleavage induced via enzymatic hydrolysis in active slurry. The  
369 various carbon isotope fractionation patterns suggest that possible several modes of hydrolytic

370 reaction are at work, implying a functional redundancy of hydrolysis. It indicates a robust  
371 degradation and possibly detoxification of phosphorodithioates in AD systems.

#### 372 **4.2.2 Hydrogen isotope fractionation**

373 Hydrogen isotope fractionations were found during the transformations of phosphorothioates.  
374 Significant hydrogen isotope fractionation of Parathion was discovered in biogas slurry system  
375 (**Table 1**). Weaker hydrogen isotope fractionation of Parathion-methyl than Parathion was  
376 observed. However, the abiotic hydrolysis of Parathion and Parathion-methyl at pH 7.0 showed  
377 no hydrogen isotope fractionation (Wu et al., 2018a). The results suggested that Parathion  
378 degradation was associated with a significant hydrogen isotope fractionation in biogas slurry  
379 caused by the dehydrogenation induced via dehydrogenase. It is assumed that dehydrogenation  
380 occurred at the sub-terminal carbon of the side chain of Parathion (C-H), giving significant  
381 hydrogen fractionation (**Table S4, SI**). Owing to the stable terminal carbon hydrogen bond of the  
382 methyl group in Parathion-methyl, it is unlikely to be attacked by dehydrogenase leading to C-H  
383 bond cleavage. We supposed that the smaller  $\epsilon_H$  of -5 and -10 in Parathion-methyl were induced  
384 via secondary hydrogen isotope effect caused by adjacent bond cleavage (Elsner et al., 2007).  
385 Since the atom was not directly involved in substitution attack, it possessed much smaller value  
386 than the primary hydrogen isotope effect (Cleland, 2003; Hennig et al., 2006; Rickert and  
387 Klinman, 1999).

#### 388 **4.2.3 Two-dimensional isotope analysis**

389 The relationship between carbon and hydrogen isotope fractionation ( $\Delta$ ) can be used to  
390 distinguish the mechanism of biotic and abiotic degradation more accurately, and this technique

391 has been adopted in several studies (Fischer et al., 2009; Palau et al., 2017; Woods et al., 2018).  
392 The substantial differences between biotic transformation and chemical hydrolysis can be  
393 visualized in the dual isotope plots (**Fig. 4** and **Fig. S17, SI**).

394 Distinct dual isotope pattern of Parathion is depicted in **Fig. 4 A**. It showed weak carbon isotope  
395 fractionation with C-O bond cleavage, diluted by P-O cleavage, and significant strong hydrogen  
396 isotope fractionation with C-H bond cleavage during transformation of Parathion in biogas slurry.  
397 The opposite pattern was discovered for chemical hydrolysis under neutral condition, showing  
398 strong isotope carbon isotope fractionation with C-O bond cleavage and lack of hydrogen isotope  
399 fractionation. Similarly, the chemical hydrolysis of Parathion-methyl conducted in neutral  
400 condition was associated with significant carbon isotope enrichment and no hydrogen isotope  
401 fractionation. Whereas strong carbon isotope fractionation via C-O bond cleavage and slight  
402 hydrogen isotope fractionation were observed in biotransformation of Parathion-methyl (**Fig. 4**  
403 **B**). The  $\Lambda$  values of Parathion in biogas slurry ( $\Lambda_{\text{original}} = 31 \pm 11$ ,  $\Lambda_{\text{cell-free}} = 20 \pm 2$ ) showed  
404 distinct pattern compared to chemical hydrolysis ( $\Lambda = 0.1 \pm 0.1$ ), as no hydrogen fractionation in  
405 abiotic hydrolysis reaction. Same trend was observed in Parathion-methyl. The value of chemical  
406 hydrolysis ( $\Lambda = -0.2 \pm 0.1$ ) was lower than in biogas slurry ( $\Lambda_{\text{original}} = 2 \pm 1$ ,  $\Lambda_{\text{cell-free}} = 1 \pm 1$ ).

407 In general, fractionation patterns of Parathion and Parathion-methyl are concordant with the  
408 assumed degradation pathways which are shown in **Scheme 1**. Hence, taking into account of the  
409 dual isotope fractionation pattern, it helps to further elucidate the proposed biotransformation  
410 pathway with the related functional enzymes and microbes in biogas slurry. Interestingly, the  
411 anaerobic degradation of Parathion using isolated strain from soil was not associated with  $^2\text{H}$  or  
412  $^{13}\text{C}$  isotope fractionation, which was assumed by reduction of the nitro groups and hydrolysis of

413 the P-O bond (Wu et al., 2018b). A low secondary hydrogen isotope effect and no significant  
414 primary carbon isotope effect was detected during reduction of nitro group of nitrobenzene  
415 (Hofstetter et al., 2008). Thus, the pronounced  $^2\text{H}$  and  $^{13}\text{C}$  fractionation indicated that reduction  
416 of nitro group was not the dominant reaction and a cleavage of a C-H bond lead to the primary  
417 isotope effect of  $^2\text{H}$  and  $^{13}\text{C}$  in the AD system. This implies that different transformation  
418 pathways under anaerobic conditions are possible and more systematic work is needed to  
419 understand the anaerobic degradation.

### 420 **4.3 Proposed reactions in biogas slurry**

#### 421 **4.3.1 Enzymatic and abiotic hydrolysis**

422 In our study Parathion was biologically transformed approximately 300 times faster than  
423 chemical hydrolysis. Similar phenomenon was also found in a mixed bacterial culture growing  
424 on Parathion and Parathion-methyl. They were hydrolyzed 2,450 times faster than conventional  
425 chemical hydrolysis (Munnecke, 1976). Hence, it was assumed to be caused by enzymatic  
426 hydrolysis, which can lead to P-O (S) cleavage at P position or C-O (S) cleavage at C position  
427 with nucleophilic attack via PTE (Serdar and Gibson, 1985; Zhang and Bennett, 2005). PTEs are  
428 a group of OP compounds degrading enzymes, which are found in microorganisms, animals and  
429 plants. The esterase, as one of the hydrolases, is the key enzyme in the first phase of biogas  
430 production (Gasch et al., 2013). Moreover, the non-specific esterase activity is suggested as  
431 indicator of bacterial heterotrophic activity in fermentation process, since the high esterase  
432 activity accompanies with increasing conversion rate of substrate to methane (Lebuhn et al.,  
433 2015). Thus, it is assumed that transformation of OPs could be caused by the  $\text{S}_{\text{N}}2$  nucleophilic  
434 substitution reaction during P-O (S) or C-O (S) bond cleavage in AD system.

### 435        **4.3.2 Dehydrogenation**

436        Significant hydrogen isotope fractionation is most likely a result of a C-H cleavage at alkyl side  
437        chain catalyzed by a dehydrogenase during biotic transformation of Parathion. Dehydrogenation  
438        was discovered in *Clostridium*, *Desulfovibrio desulfuricans* and a *Bacteroides* sp. via  
439        dehydrogenase in anaerobic pathway (Dwyer and Tiedje, 1986; Kocholaty and Hoogerheide,  
440        1938; Zhang and Bennett, 2005). Aliphatic hydrocarbons and alkyl groups of aromatic  
441        hydrocarbons are activated by dehydrogenase reactions under anoxic conditions (Musat et al.,  
442        2016). The large diversity of bacteria in AD system (Qiao et al., 2013; Weiland, 2010) suggested  
443        that certain strains may be capable of dehydrogenation, such as *Clostridium* sp. Moreover,  
444        several studies had already reported that microbes in biogas plants possess dehydrogenase  
445        (Lebuhn et al., 2008; Maus et al., 2017; Rotaru et al., 2014) and dual C-H isotope analysis could  
446        be used to show their activity in degradation. Moreover, the tentative identification of diethyl  
447        (2E)-2-butenedioate (**Fig. S7, SI**) as the metabolite of Malathion gave also a hint for the  
448        dehydrogenation in biogas slurry.

### 449        **4.3.3 Reduction of the nitro group**

450        Amino-parathion and amino-parathion-methyl were found in biogas slurry system, which gave  
451        direct evidence for reduction mechanism. This reaction will not contribute to carbon or hydrogen  
452        isotope fractionation. The reductive transformation of Parathion and Parathion-methyl by  
453        *Bacillus* sp. was also investigated in a former study (Yang et al., 2007).

## 454        **5. Conclusion**

455 OP can be transformed by different reaction modes in the AD system. The varying isotope  
456 fractionation pattern illustrated coexistence of different modes of hydrolytic activities, implying  
457 the functional redundancies of enzymes in biogas slurry and suggesting that AD systems provide  
458 robust degradation capacity for OP transformation. The cell-free experiments showed variety of  
459 enzymatic activities which were partly bound to enzymes resident to higher temperature, as  
460 tested in heat sterilized experiment. Very interesting is that the different modes of hydrolytic  
461 activities in AD are capable to degrade OPs efficiently. Consequently, in AD condition, most  
462 OPs can be degraded rapidly and biogas process could be a promising remediation measure for  
463 the biomass from contaminated field sites or organic rich waste materials. Thus, this study  
464 promotes the investigation on the fate of OPs in the environment, providing a new remediation  
465 method for the contaminated biomass and illustrating different pathways of biotic and abiotic  
466 transformations via 2D-CSIA.

#### 467 **Supporting information**

468 E-supplementary data (Supporting Information) for this work can be found in e-version of this  
469 paper online.

#### 470 **Acknowledgements**

471 Shujuan Lian [File No. 201404910520] and Langping Wu [File No. 201306460007] were funded  
472 by the China Scholarship Council and supported by the Helmholtz Interdisciplinary Graduate  
473 School for Environmental Research. The active biogas slurry was supplied by DBFZ (German  
474 Biomass Research Centre). We thank Steffen Kümmel and Ursula Günther for helping with  
475 isotope measurements. And we also would like to give thanks to Jan Kaesler and Bettina Seiwert

476 for helping with FT-ICR MS and LC-MS measurements. The study was supported by the  
477 Initiative and Networking Fund of the Helmholtz Association.

478

479 **References**

- 480 Adhya, T.K., Barik, S., Sethunathan, N., 1981. Fate of fenitrothion, methyl parathion, and  
481 parathion in anoxic sulfur-containing soil systems. *Pestic. Biochem. Physiol.* 16, 14–20.
- 482 Azmy, A.F., Saafan, A.E., Essam, T.M., Amin, M.A., Ahmed, S.H., 2015. Biodegradation of  
483 malathion by *Acinetobacter baumannii* strain AFA isolated from domestic sewage in Egypt.  
484 *Int. Sch. Sci. Res. Innov.* 9, 55–65.
- 485 Barton, J.W., Kuritz, T., O'Connor, L.E., Ma, C.Y., Maskarinec, M.P., Davison, B.H., 2004.  
486 Reductive transformation of methyl parathion by the cyanobacterium *Anabaena* sp. strain  
487 PCC7120. *Appl. Microbiol. Biotechnol.* 65, 330–335.
- 488 Battersby, N.S., Wilson, V., 1989. Survey of the anaerobic biodegradation potential of organic  
489 chemicals in digesting sludge. *Appl. Environ. Microbiol.* 55, 433–439.
- 490 Brock, T.D., 1985. Life at high temperatures. *Science.* 230, 132–138.
- 491 Chanda, A., Khetan, S.K., Banerjee, D., Ghosh, A., Collins, T.J., 2006. Total degradation of  
492 fenitrothion and other organophosphorus pesticides by catalytic oxidation employing Fe-  
493 TAML peroxide activators. *J. Am. Chem. Soc.* 128, 12058–12059.
- 494 Cleland, W.W., 2003. The use of isotope effects to determine enzyme mechanisms. *J. Biol.*  
495 *Chem.* 278, 51975–51984.
- 496 Coplen, T.B., Brand, W.A., Gehre, M., Groning, M., Meijer, H.A.J., Toman, B., Verkouteren,  
497 R.M., 2006. New guidelines for  $\delta^{13}\text{C}$  measurements. *Anal. Chem.* 78, 2439–2441.

498 Ding, J., Shen, X., Liu, W., Covaci, A., Yang, F., 2015. Occurrence and risk assessment of  
499 organophosphate esters in drinking water from Eastern China. *Sci. Total Environ.* 538, 959–  
500 965.

501 Druzina, B., Stegu, M., 2007. Degradation study of selected organophosphorus insecticides in  
502 natural waters. *Int. J. Environ. Anal. Chem.* 87, 1079–1093.

503 Dwyer, D.F., Tiedje, J.M., 1986. Metabolism of polyethylene glycol by two anaerobic bacteria.  
504 *Appl. Environ. Microbiol.* 52, 852–856.

505 Elsner, M., Mckelvie, J., Couloume, G.L., Lollar, B.S., 2007. Insight into Methyl tert-Butyl  
506 Ether (MTBE) stable isotope fractionation from abiotic reference experiments. *Environ. Sci.*  
507 *Technol.* 41, 5693–5700.

508 Fischer, A., Gehre, M., Breitfeld, J., Richnow, H.H., Vogt, C., 2009. Carbon and hydrogen  
509 isotope fractionation of benzene during biodegradation under sulfate-reducing conditions: a  
510 laboratory to field site approach. *Rapid Commun. Mass Spectrom.* 23, 2439–2447.

511 Gasch, C., Hildebrandt, I., Rebbe, F., Röske, I., 2013. Enzymatic monitoring and control of a  
512 two-phase batch digester leaching system with integrated anaerobic filter. *Energy. Sustain.*  
513 *Soc.* 3, 1–11.

514 Gehre, M., Renpenning, J., Gilevska, T., Qi, H., Coplen, T.B., Meijer, H.A.J., Brand, W.A.,  
515 Schimmelmann, A., 2015. On-line hydrogen-isotope measurements of organic samples  
516 using elemental chromium: an extension for high temperature elemental-analyzer  
517 techniques. *Anal. Chem.* 87, 5198–5205.

518 Graetz, D.A., Chesters, G., Daniel, T.C., Newland, L.W., Lee, G.B., 1970. Parathion degradation  
519 in lake sediments. *Water Pollut. Control Fed.* 42, R76–R94.

520 Guo, X., Jans, U., 2006. Kinetics and mechanism of the degradation of methyl parathion in  
521 aqueous hydrogen sulfide solution: investigation of natural organic matter effects. *Environ.*  
522 *Sci. Technol.* 40, 900–906.

523 Hennig, C., Oswald, R.B., Schmatz, S., 2006. Secondary kinetic isotope effect in nucleophilic  
524 substitution: a quantum-mechanical approach. *J. Phys. Chem. A* 110, 3071–3079.

525 Hofstetter, T.B., Schwarzenbach, R.P., Bernasconi, S.M., 2008. Assessing transformation  
526 processes of organic compounds using stable isotope fractionation. *Environ. Sci. Technol.*  
527 42, 7737–7743.

528 Karami-Mohajeri, S., Abdollahi, M., 2010. Toxic influence of organophosphate, carbamate, and  
529 organochlorine pesticides on cellular metabolism of lipids, proteins, and carbohydrates: a  
530 systematic review. *Hum. Exp. Toxicol.* 30, 1119–1140.

531 Katan, J., Fuhremann, T.W., Lichtenstein, E.P., 1976. Binding of (<sup>14</sup>C) parathion in soil: a  
532 reassessment of pesticide persistence. *Science.* 193, 891–894.

533 Kocholaty, W., Hoogerheide, J.C., 1938. Studies of the metabolism of the strict anaerobes (genus  
534 *Clostridium*) I. dehydrogenation reactions by suspensions of *Cl. sporogenes*. *Biol. Rev.* 13,  
535 437–448.

536 Kupper, T., Bucheli, T.D., Brändli, R.C., Ortelli, D., Edder, P., 2008. Dissipation of pesticides

537 during composting and anaerobic digestion of source-separated organic waste at full-scale  
538 plants. *Bioresour. Technol.* 99, 7988–7994.

539 Lacorte, S., Lartinges, S.B., Garrigues, P., Barcelo, D., 1995. Degradation of organophosphorus  
540 pesticides and their transformation products in estuarine waters. *Environ. Sci. Technol.* 29,  
541 431–438.

542 Lebuhn, M., Liu, F., Heuwinkel, H., Gronauer, A., 2008. Biogas production from mono-  
543 digestion of maize silage-long-term process stability and requirements. *Water Sci. Technol.*  
544 58, 1645–1651.

545 Lebuhn, M., Weiß, S., Munk, B., Guebitz, G.M., 2015. Microbiology and molecular biology  
546 tools for biogas process analysis, diagnosis and control, in: Guebitz, G.M., Bauer, A.,  
547 Bochmann, G., Gronauer, A., Weiß, S. (Eds.), *Biogas Science and Technology*. Springer  
548 International Publishing, Cham, pp. 1–40.

549 Li, L., Yang, C., Lan, W., Xie, S., Qiao, C., Liu, J., 2008. Removal of methyl parathion from  
550 artificial off-gas using a bioreactor containing a constructed microbial consortium. *Environ.*  
551 *Sci. Technol.* 42, 2136–2141.

552 Lian, S., Nikolausz, M., Nijenhuis, I., Leite, A.F., Richnow, H.H., 2018. Biotransformation and  
553 inhibition effects of hexachlorocyclohexanes during biogas production from contaminated  
554 biomass characterized by isotope fractionation concepts. *Bioresour. Technol.* 250, 683–690.

555 Liu, Y.H., Chung, Y.C., Xiong, Y., 2001. Purification and characterization of a dimethoate-  
556 degrading enzyme of *Aspergillus niger* ZHY256, isolated from sewage. *Appl. Environ.*

557 Microbiol. 67, 3746–3749.

558 Mariotti, A., Germon, J.C., Hubert, P., Kaiser, P., Letolle, R., Tardieux, A., Tardieux, P., 1981.  
559 Experimental determination of nitrogen kinetic isotope fractionation: some principles;  
560 illustration for the denitrification and nitrification processes. *Plant Soil* 62, 413–430.

561 Maus, I., Bremges, A., Stolze, Y., Hahnke, S., Cibis, K.G., Koeck, D.E., Kim, Y.S., Kreubel, J.,  
562 Hassa, J., Wibberg, D., Weimann, A., Off, S., Stantscheff, R., Zverlov, V. V., Schwarz,  
563 W.H., König, H., Liebl, W., Scherer, P., McHardy, A.C., Sczyrba, A., Klocke, M., Pühler,  
564 A., Schlüter, A., 2017. Genomics and prevalence of bacterial and archaeal isolates from  
565 biogas-producing microbiomes. *Biotechnol. Biofuels* 10, 1–22.

566 Meyer, A.H., Penning, H., Elsner, M., 2009. C and N isotope fractionation suggests similar  
567 mechanisms of microbial atrazine transformation despite involvement of different enzymes  
568 (AtzA and TrzN). *Environ. Sci. Technol.* 43, 8079–8085.

569 Monsalvo, V.M., Garcia-Mancha, N., Puyol, D., Mohedano, A.F., Rodriguez, J.J., 2014.  
570 Anaerobic biodegradability of mixtures of pesticides in an expanded granular sludge bed  
571 reactor. *Water Sci. Technol.* 69, 532–538.

572 Munnecke, D.M., 1976. Enzymatic hydrolysis of organophosphate insecticides, a possible  
573 pesticide disposal method. *Appl. Environ. Microbiol.* 32, 7–13.

574 Musat, F., Vogt, C., Richnow, H.H., 2016. Carbon and hydrogen stable isotope fractionation  
575 associated with the aerobic and anaerobic degradation of saturated and alkylated aromatic  
576 hydrocarbons. *J. Mol. Microbiol. Biotechnol.* 26, 211–226.

577 Palau, J., Yu, R., Hatijah Mortan, S., Shouakar-Stash, O., Rosell, M., Freedman, D.L., Sbarbati,  
578 C., Fiorenza, S., Aravena, R., Marco-Urrea, E., Elsner, M., Soler, A., Hunkeler, D., 2017.  
579 Distinct dual C-Cl isotope fractionation patterns during anaerobic biodegradation of 1,2-  
580 dichloroethane: potential to characterize microbial degradation in the field. *Environ. Sci.*  
581 *Technol.* 51, 2685–2694.

582 Pang, L., Ge, L., Yang, P., He, H., Zhang, H., 2018. Degradation of organophosphate esters in  
583 sewage sludge: effects of aerobic/anaerobic treatments and bacterial community  
584 compositions. *Bioresour. Technol.* 255, 16–21.

585 Penning, H., Sørensen, S.R., Meyer, A.H., Aamand, J., Elsner, M., 2010. C, N, and H isotope  
586 fractionation of the herbicide isoproturon reflects different microbial transformation  
587 pathways. *Environ. Sci. Technol.* 44, 2372–2378.

588 Peuke, A.D., Rennenberg, H., 2005. Phytoremediation. *EMBO Rep.* 6, 497–501.

589 Qiao, J.T., Qiu, Y.L., Yuan, X.Z., Shi, X.S., Xu, X.H., Guo, R.B., 2013. Molecular  
590 characterization of bacterial and archaeal communities in a full-scale anaerobic reactor  
591 treating corn straw. *Bioresour. Technol.* 143, 512–518.

592 Rayleigh, L., 1896. Theoretical considerations respecting the separation of gases by diffusion  
593 and similar processes. *London, Edinburgh, Dublin Philos. Mag. J. Sci.* 42, 493–498.

594 Reemtsma, T., Quintana, J.B., Rodil, R., Garcia-Lopez, M., Rodriguez, I., 2008.  
595 Organophosphorus flame retardants and plasticizers in water and air I. Occurrence and fate.  
596 *Trends Anal. Chem.* 27, 727–737.

- 597 Renpenning, J., Kümmel, S., Hitzfeld, K.L., Schimmelmann, A., Gehre, M., 2015. Compound-  
598 specific hydrogen isotope analysis of heteroatom-bearing compounds via gas  
599 chromatography-chromium-based high-temperature conversion (Cr/HTC)-isotope ratio  
600 mass spectrometry. *Anal. Chem.* 87, 9443–9450.
- 601 Rickert, K.W., Klinman, J.P., 1999. Nature of hydrogen transfer in soybean lipoxygenase 1:  
602 separation of primary and secondary isotope effects. *Biochemistry* 38, 12218–12228.
- 603 Rotaru, A.E., Shrestha, P.M., Liu, F., Shrestha, M., Shrestha, D., Embree, M., Zengler, K.,  
604 Wardman, C., Nevin, K.P., Lovley, D.R., 2014. A new model for electron flow during  
605 anaerobic digestion: direct interspecies electron transfer to *Methanosaeta* for the reduction  
606 of carbon dioxide to methane. *Energy Environ. Sci.* 7, 408–415.
- 607 Serdar, C.M., Gibson, D.T., 1985. Enzymetic hydrolysis of organophosphates: cloning and  
608 expression of a parathion hydrolase gene from *Pseudomonas Diminuta*. *Nat. Biotechnol.* 3,  
609 567–571.
- 610 Singh, B.K., 2009. Organophosphorus-degrading bacteria: ecology and industrial applications.  
611 *Nat. Rev. Microbiol.* 7, 156–164.
- 612 Singh, B.K., Walker, A., 2006. Microbial degradation of organophosphorus compounds. *FEMS*  
613 *Microbiol. Rev.* 30, 428–471.
- 614 Singh, B.K., Walker, A., Wright, D.J., 2005. Cross-enhancement of accelerated biodegradation  
615 of organophosphorus compounds in soils: dependence on structural similarity of compounds.  
616 *Soil Biol. Biochem.* 37, 1675–1682.

617 Sogorb, M.A., Vilanova, E., 2002. Enzymes involved in the detoxification of organophosphorus,  
618 carbamate and pyrethroid insecticides through hydrolysis. *Toxicol. Lett.* 128, 215–228.

619 Theriot, C.M., Grunden, A.M., 2011. Hydrolysis of organophosphorus compounds by microbial  
620 enzymes. *Appl. Microbiol. Biotechnol.* 89, 35–43.

621 Van den Eede, N., Maho, W., Erratico, C., Neels, H., Covaci, A., 2013. First insights in the  
622 metabolism of phosphate flame retardants and plasticizers using human liver fractions.  
623 *Toxicol. Lett.* 223, 9–15.

624 Wanamaker, E.C., Chingas, G.C., McDougal, O.M., 2013. Parathion hydrolysis revisited: in situ  
625 aqueous kinetics by  $^1\text{H}$  NMR. *Environ. Sci. Technol.* 47, 9267–9273.

626 Weiland, P., 2010. Biogas production: current state and perspectives. *Appl. Microbiol.*  
627 *Biotechnol.* 85, 849–860.

628 Woods, A., Kuntze, K., Gelman, F., Halicz, L., Nijenhuis, I., 2018. Variable dual carbon-  
629 bromine stable isotope fractionation during enzyme-catalyzed reductive dehalogenation of  
630 brominated ethenes. *Chemosphere* 190, 211–217.

631 Wu, L., Chládková, B., Lechtenfeld, O.J., Lian, S., Schindelka, J., Herrmann, H., Richnow, H.H.,  
632 2018a. Characterizing chemical transformation of organophosphorus compounds by  $^{13}\text{C}$  and  
633  $^2\text{H}$  stable isotope analysis. *Sci. Total Environ.* 615, 20–28.

634 Wu, L., Kümmel, S., Richnow, H.H., 2017. Validation of GC–IRMS techniques for  $\delta^{13}\text{C}$  and  
635  $\delta^2\text{H}$  CSIA of organophosphorus compounds and their potential for studying the mode of

636 hydrolysis in the environment. *Anal. Bioanal. Chem.* 409, 2581–2590.

637 Wu, L., Verma, D., Bondgaard, M., Melvej, A., Vogt, C., Subudhi, S., Richnow, H.H., 2018b.  
638 Carbon and hydrogen isotope analysis of parathion for characterizing its natural attenuation  
639 by hydrolysis at a contaminated site. *Water Res.* 143, 146–154.

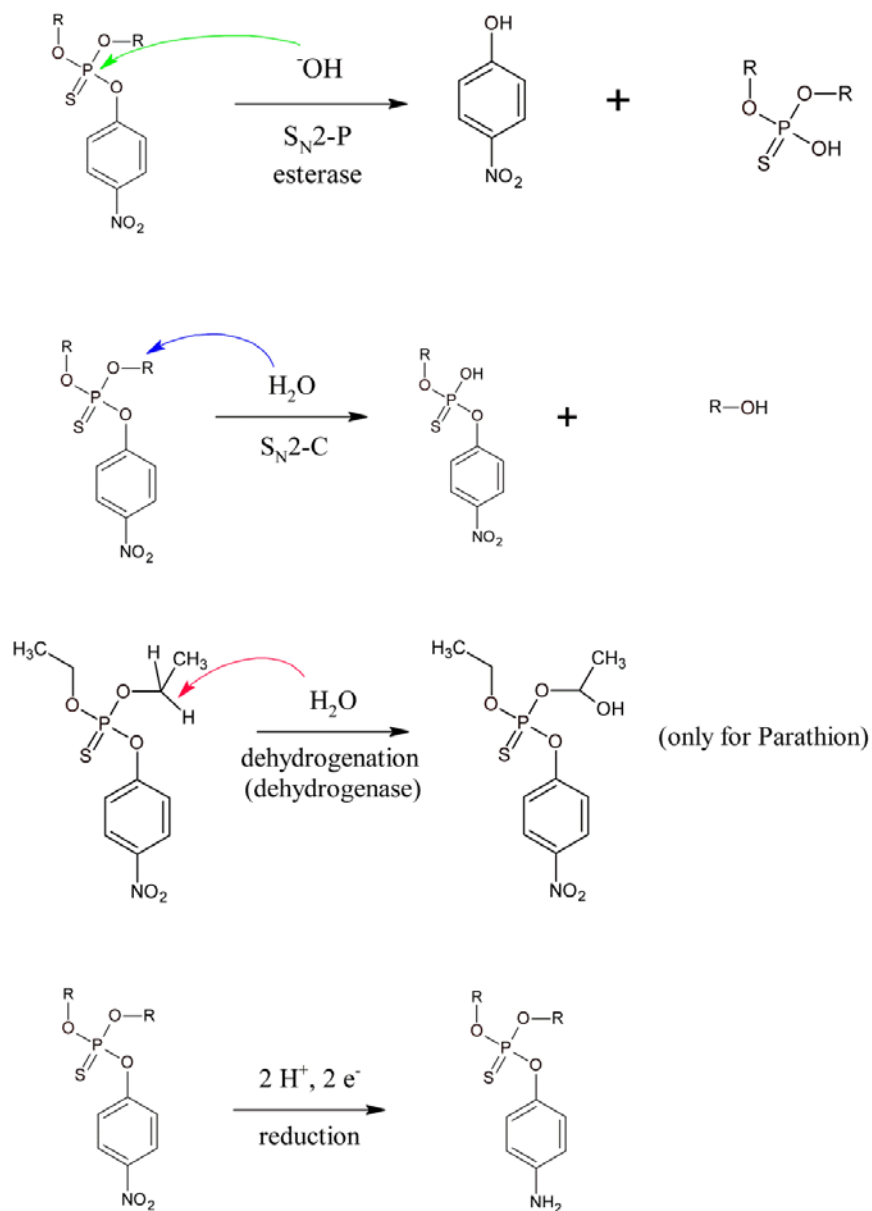
640 Wu, L., Yao, J., Trebse, P., Zhang, N., Richnow, H.H., 2014. Compound specific isotope  
641 analysis of organophosphorus pesticides. *Chemosphere* 111, 458–463.

642 Yang, C., Dong, M., Yuan, Y., Huang, Y., Guo, X., Qiao, C., 2007. Reductive transformation of  
643 parathion and methyl parathion by *Bacillus* sp. *Biotechnol. Lett.* 29, 487–493.

644 Zhang, C., Bennett, G.N., 2005. Biodegradation of xenobiotics by anaerobic bacteria. *Appl.*  
645 *Microbiol. Biotechnol.* 67, 600–618.

646 Zhang, N., Schindelka, J., Herrmann, H., George, C., Rosell, M., Herrero-Martín, S., Klán, P.,  
647 Richnow, H.H., 2015. Investigation of humic substance photosensitized reactions via  
648 carbon and hydrogen isotope fractionation. *Environ. Sci. Technol.* 49, 233–242.

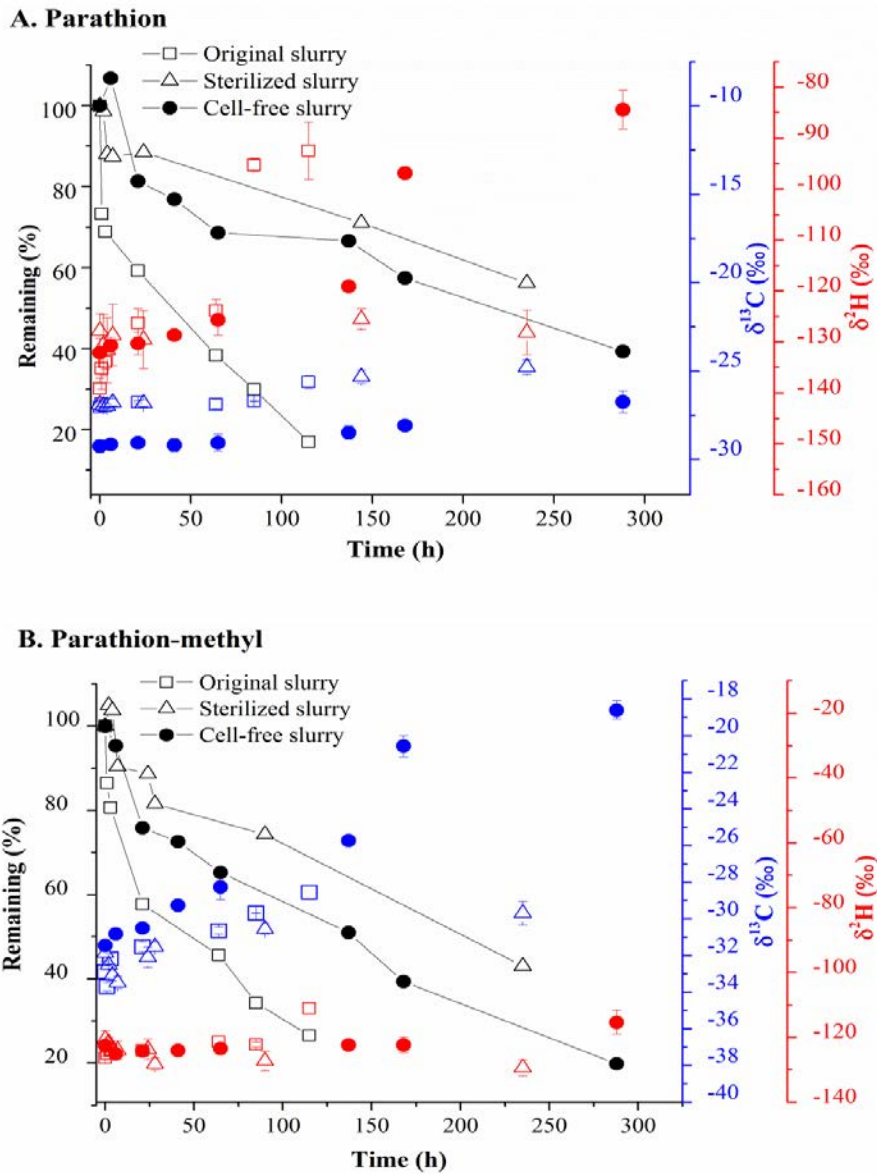
Enzymatic hydrolysis of Parathion (R = C<sub>2</sub>H<sub>5</sub>) and Parathion-methyl (R = CH<sub>3</sub>)



649 **Scheme 1.** Proposed transformation pathways of Parathion and Parathion-methyl in biogas slurry

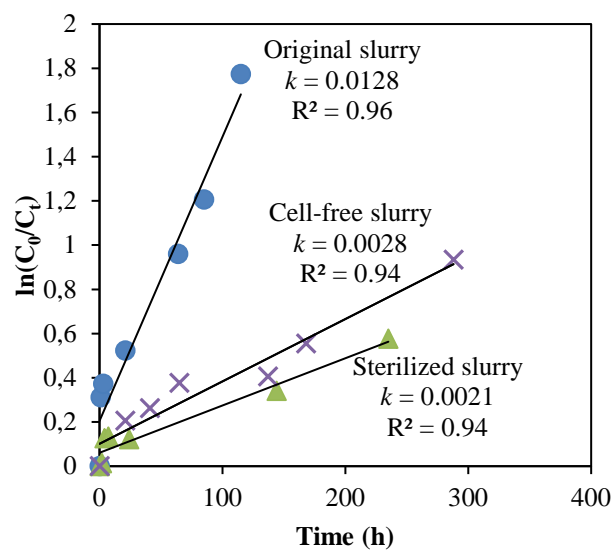
650

651

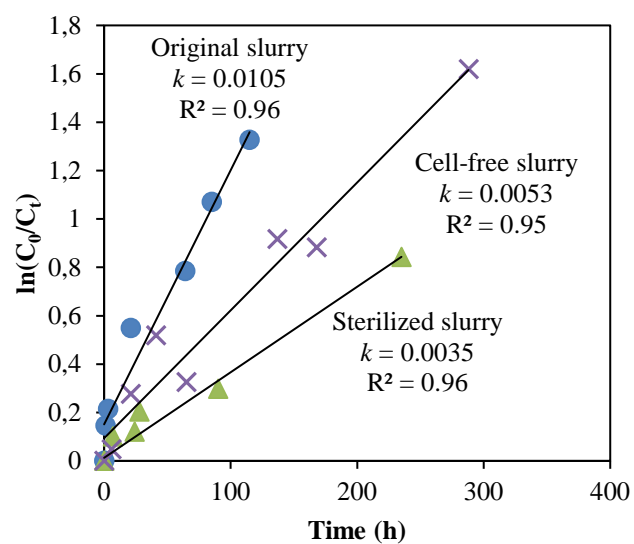


653 **Fig. 1.** Concentration of the remaining fractions (black symbols), and stable isotope  
 654 compositions (blue =  $^{13}\text{C}$  / red =  $^2\text{H}$ ) of Parathion (A) and Parathion-methyl (B). The isotope  
 655 composition of experiments with original slurry, cell-free slurry and sterilized slurry are  
 656 represented by empty square ( $\square$ ), dark circle ( $\bullet$ ) and empty triangle ( $\triangle$ ), respectively.

### A. Parathion

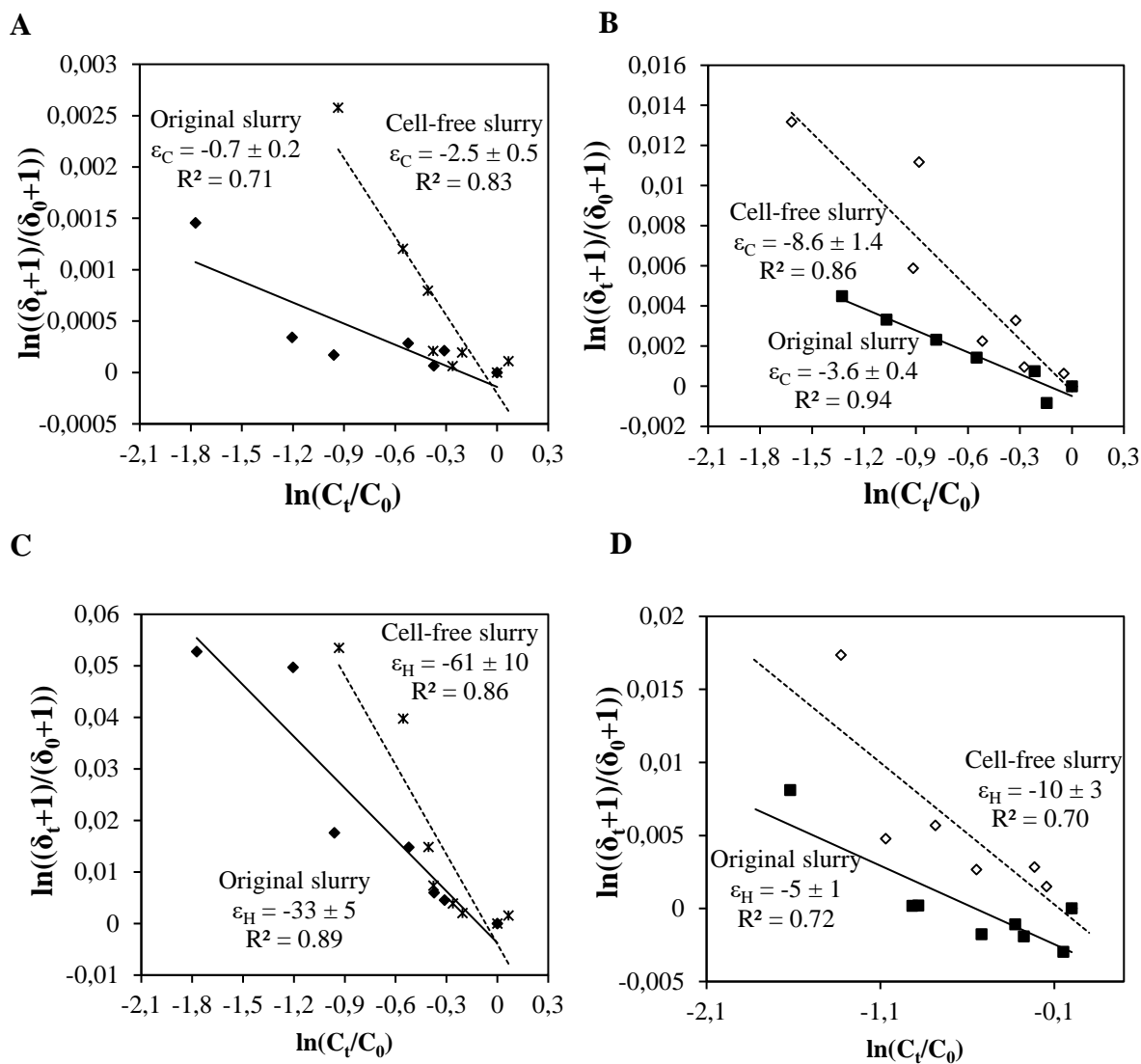


### B. Parathion-methyl



657

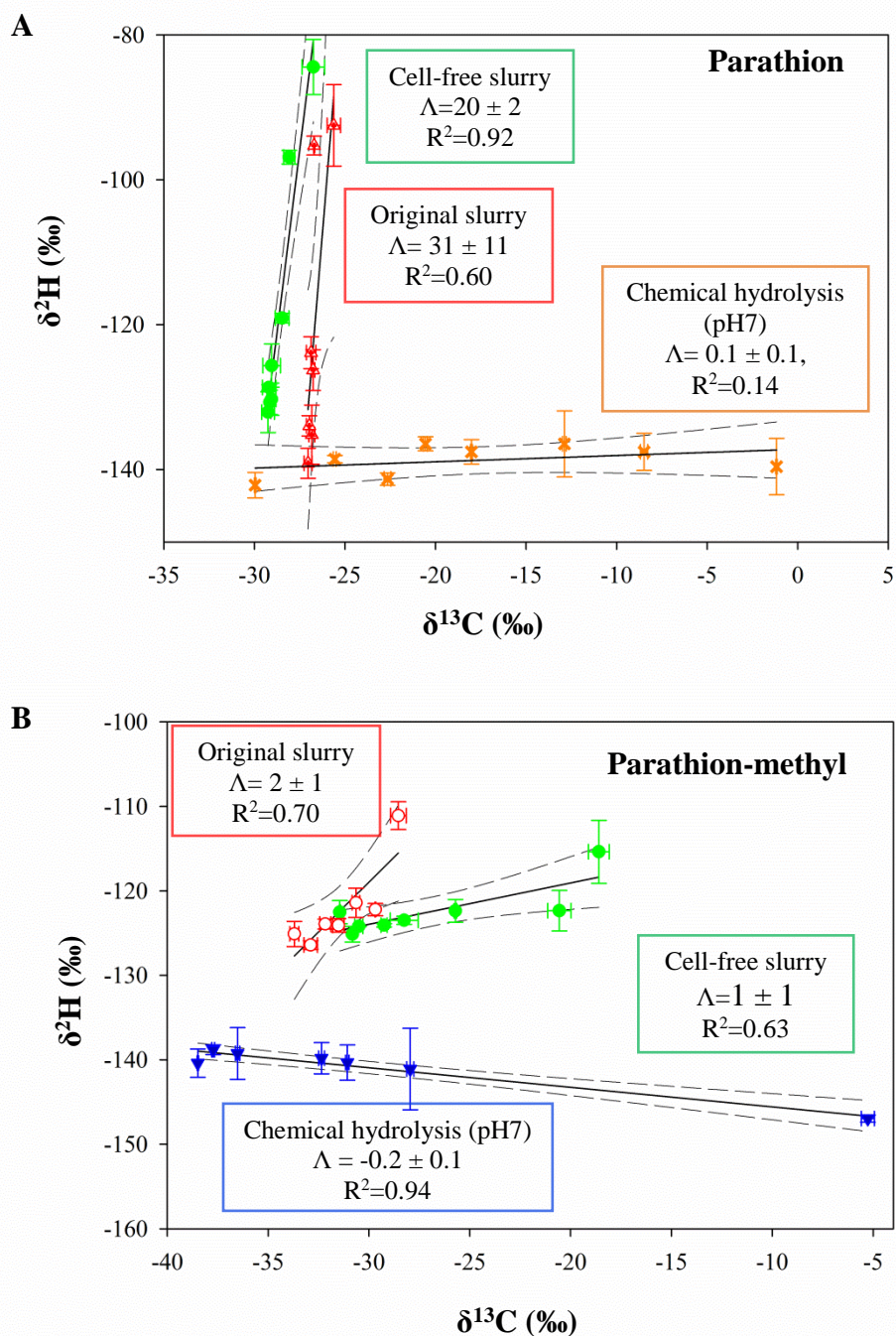
658 **Fig. 2.** First order rate constants of Parathion (A) and Parathion-methyl (B) degradation in biogas  
659 slurry.



660

661 **Fig. 3.** Carbon and hydrogen enrichment factors of Parathion (A&C) and Parathion-methyl  
 662 (B&D) during transformations in original biogas slurry and cell-free slurry.

663



664 **Fig. 4.** 2D-CSIA plots of Parathion (A) and Parathion-methyl (B) for comparing enzymatic  
 665 hydrolysis in biogas slurry with abiotic hydrolysis. Dashed lines are linear regressions with 95%  
 666 confidential intervals.

**Table 1** Carbon/hydrogen isotopic enrichment factors ( $\epsilon$ ) and two dimensional plot- $\Lambda$  values of OPs degradation in AD process.

Compounds	Reactions	T(°C)	$\kappa$ ( $\times 10^{-3}$ h <sup>-1</sup> )	t <sub>1/2</sub> (h)	$\epsilon_C \pm 95\%CI$ (‰)	R <sup>2</sup>	$\epsilon_H \pm 95\%CI$ (‰)	R <sup>2</sup>	$\Lambda$	
<b>Parathion</b>	<b>Original slurry</b> (50-fold dilution)	37	12.8 ± 1.2	54	-0.7 ± 0.2	0.71	-33 ± 5	0.89	31 ± 11	
	<b>Cell-free slurry</b> (50-fold dilution)	37	2.8 ± 0.3	247	-2.5 ± 0.5	0.83	-61 ± 10	0.86	20 ± 2	
	<b>Sterilized slurry</b> (50-fold dilution)	37	2.1 ± 0.2	330	-4.3 ± 0.4	0.98	nf			
	aerobic strains TERI OP1*	30	71.4 ± 14.5	9.7	nf		nf			
	aerobic strains TERI OP2*	30	35.1 ± 8.5	19.7	nf		nf			
	anaerobic strain TERI ANA-1*	30	19.4 ± 1.8	35.7	nf		nf			
	Chemical hydrolysis*	pH 2	60		70.1	-6.9 ± 0.8	0.99	nf		
		pH 5	60		71.8	-6.7 ± 0.4	0.99	nf		
		pH 7	60		74.9	-6.0 ± 0.2	0.99	nf		
		pH 9	60		49.5	-3.5 ± 0.4	0.99	nf		
	pH 12	20		27.3	nf		nf			
<b>Parathion-methyl</b>	<b>Original slurry</b> (50-Fold dilution)	37	10.5 ± 1.0	66	-3.6 ± 0.4	0.94	-5 ± 1	0.72	2 ± 1	
	<b>Cell-free slurry</b> (50-fold dilution)	37	5.3 ± 0.5	131	-8.6 ± 1.4	0.86	-10 ± 3	0.70	1 ± 1	
	<b>Sterilized slurry</b> (50-fold dilution)	37	3.5 ± 0.3	198	-10.3 ± 0.1	0.99	nf			
	Chemical hydrolysis*	pH 2	60		23.2	-10.0 ± 0.7	0.99	nf		
		pH 5	60		17.3	-10.5 ± 1.1	0.99	nf		
		pH 7	60		16.2	-9.9 ± 0.7	0.99	nf		
		pH 9	60		13.0	-6.5 ± 0.4	0.98	nf		
	pH 12	20		3.7	nf		nf			
<b>Dimethoate</b>	<b>Original slurry</b> (5-fold dilution)	37	39.6 ± 7.9	13.7	-0.6 ± 0.1	0.87	nf			
	<b>Cell-free slurry</b> (5-fold dilution)	37	33.3 ± 5.5	20.8	-0.9 ± 0.1	0.93				
	<b>Sterilized slurry</b> (5-fold dilution)	37	14.8 ± 3.5	46.8	-1.6 ± 0.4	0.86				
	Hydro_pH7*	60		37.7	-8.3 ± 0.3	0.99	nf			
	Hydro_pH9*	30		56.3	-1.4 ± 0.1	0.98	-10 ± 3	0.92		
<b>Malathion</b>	<b>Original slurry</b> (5-fold dilution)	37	50.5 ± 5.3	17.5	-5.5 ± 0.1	0.99	nf			
	<b>Cell-free slurry</b> (5-fold dilution)	37	35.5 ± 6.7	19.5	-7.2 ± 0.5	0.99				
<b>TCEP</b>	<b>Original slurry</b> (25-fold dilution)	37	3.1 ± 0.5	223	nf		nf			
	<b>Cell-free slurry</b> (25-fold dilution)	37	0.8 ± 0.1	866	nf		nf			
	UV/H <sub>2</sub> O <sub>2</sub> *	20		2.6	-1.4 ± 0.1	0.99	-56 ± 3	0.99		
<b>TDCPP</b>	<b>Original slurry</b> (25-fold dilution)	37	2.6 ± 0.4	266	nf		nf			
	<b>Cell-free slurry</b> (25-fold dilution)	37	2.4 ± 0.3	289	nf		nf			

\*: Data were derived from hydrolysis tests and reported by Wu *et al* (Wu et al., 2018a, 2018b); nd: no degradation; nf: no fractionation.

1 **Supporting information to**

2  **$^2\text{H}$  and  $^{13}\text{C}$  isotope fractionation analysis of organophosphorus compounds for**  
3 **characterizing transformation reactions in biogas slurry: Potential for anaerobic**  
4 **treatment of contaminated biomass**

5  
6 Shujuan Lian<sup>1</sup>, Langping Wu<sup>1</sup>, Marcell Nikolausz<sup>2</sup>, Oliver J. Lechtenfeld<sup>3</sup>, Hans H. Richnow<sup>1\*</sup>

7 <sup>1</sup> Department of Isotope Biogeochemistry, Helmholtz Centre for Environmental Research-UFZ,  
8 Permoserstraße 15, 04318 Leipzig, Germany

9 <sup>2</sup> Department of Environmental Microbiology, Helmholtz Centre for Environmental Research-  
10 UFZ, Permoserstraße 15, 04318 Leipzig, Germany

11 <sup>3</sup>Department of Analytical Chemistry, Helmholtz Centre for Environmental Research-UFZ,  
12 Permoserstraße 15, 04318 Leipzig, Germany

13 shujuan.lian@ufz.de

14 langping.wu@ufz.de

15 marcell.nikolausz@ufz.de

16 oliver.lechtenfeld@ufz.de

17  
18 \*Corresponding author. Tel.: +49 341 2351 212; fax: +49 341 451 212. E-mail address:

19 hans.richnow@ufz.de

20 **Contents**

21 Supporting information to..... 1

22 S1. Characteristics of organophosphate ester derivatives (OPs) ..... 3

23 S2. Methods ..... 5

24 S2.1. Deactivation of the GC glass liner..... 5

25 S2.2. Extraction..... 5

26 S3. Biotransformation of OPs ..... 6

27 S3.1. Transformation of OPs in biogas slurry..... 6

28 S3.2. Isotope fractionation of OPs in biogas slurry ..... 10

29 S4. Identification of metabolites by GC-MS ..... 11

30 S5. Characterization of metabolites by FT-ICR MS..... 15

31 S5.1. Preparation of samples..... 15

32 S5.2. Identified metabolites ..... 16

33 S6. 2D-plot for TCEP, TDCPP, Dimethoate and Malathion ..... 34

34 S7. Methylation as subsequent reaction..... 36

35 References..... 37

36

37

38

39 **S1. Characteristics of organophosphate ester derivatives (OPs)**

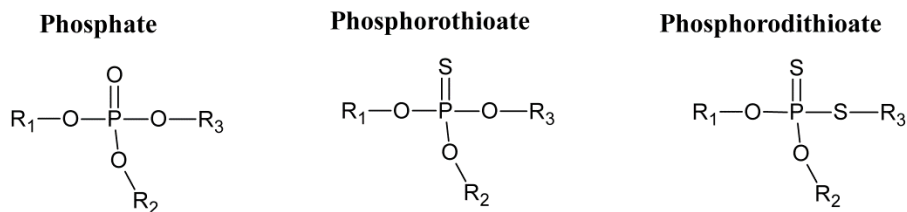
40 **Table S1** Chemical properties of OPs

	Solubility in water <sup>#</sup>	Density (g mL <sup>-1</sup> ) <sup>#</sup>	Molar mass (g mol <sup>-1</sup> ) <sup>#</sup>	Boiling point (°C) <sup>#</sup>	Chemical formula	Initial concentration in this study*	$\kappa$ (( $\times 10^{-3}$ h <sup>-1</sup> ) in biogas slurry without dilution (estimated value) *
<b>Phosphate</b>							
TCEP	7.82 g L <sup>-1</sup>	1.39	285.48	192	C <sub>6</sub> H <sub>12</sub> Cl <sub>3</sub> O <sub>4</sub> P	12 mg L <sup>-1</sup>	141
TDCPP	18.1 mg L <sup>-1</sup>	1.514	430.91	326	C <sub>9</sub> H <sub>15</sub> C <sub>16</sub> O <sub>4</sub> P	5 mg L <sup>-1</sup>	158
<b>Phosphorothioate</b>							
Parathion	24 mg L <sup>-1</sup>	1.27	291.3	375	C <sub>10</sub> H <sub>14</sub> NO <sub>5</sub> P S	12 mg L <sup>-1</sup>	2.8 $\times 10^3$
Parathion-methyl	50 mg L <sup>-1</sup>	1.358	263.21	154	C <sub>8</sub> H <sub>10</sub> NO <sub>5</sub> PS	25 mg L <sup>-1</sup>	2.3 $\times 10^3$
<b>Phosphorodithioate</b>							
Dimethoate	25 g L <sup>-1</sup>	1.3	229.26	117	C <sub>5</sub> H <sub>12</sub> NO <sub>3</sub> PS 2	100 mg L <sup>-1</sup>	288
Malathion	145 mg L <sup>-1</sup>	1.23	330.36	156	C <sub>10</sub> H <sub>19</sub> O <sub>6</sub> PS <sub>2</sub>	25 mg L <sup>-1</sup>	217

41 <sup>#</sup>: Data were taken from <https://www.wikipedia.org/>.

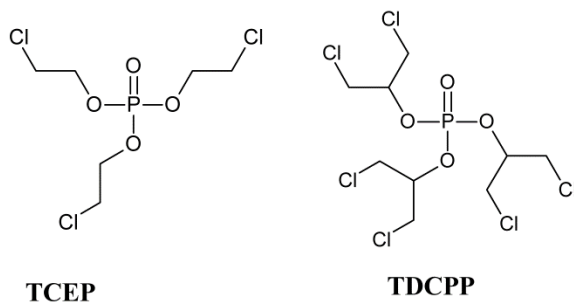
42 <sup>\*</sup>: concentrations were decided based on solubility in water and kinetic constants were estimated from experimental data.

43 **Scheme S1.** Chemical structures of OPs included in present study.

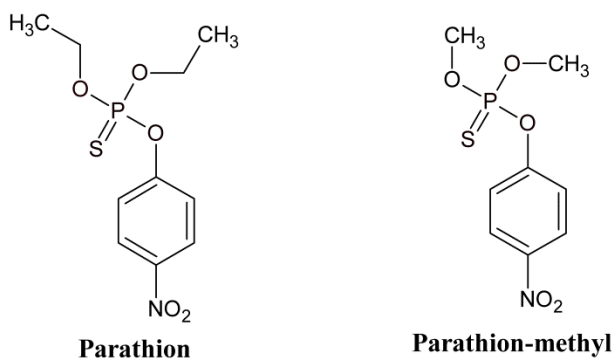


(R<sub>1</sub> and R<sub>2</sub> are predominantly aryl or alkyl group. R<sub>3</sub> can be diverse and may belong to a wide range of aliphatic, aromatic or heterocyclic group.)

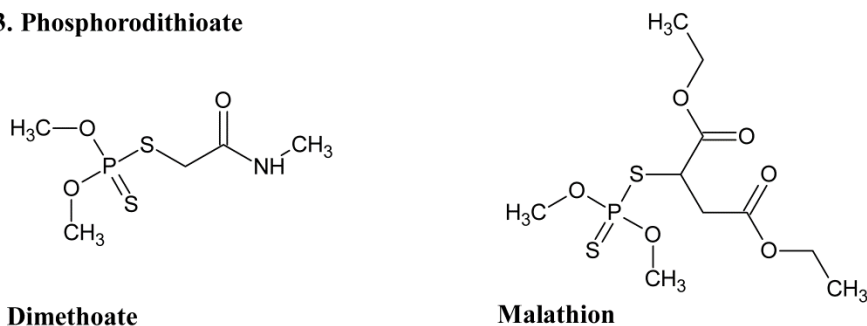
**1. Phosphate**



**2. Phosphorothioate**



**3. Phosphorodithioate**



## 45 **S2. Methods**

### 46 **S2.1. Deactivation of the GC glass liner**

47 Our previous study showed that the performance of glass liner used for split/splitless injection  
48 into GC is critical for precise isotope analytics (Wu et al., 2014). Poor inertness of the liner led to  
49 significant shifts on  $\delta^{13}\text{C}$  and  $\delta^2\text{H}$  values and showed an unconventional linearity range, due to  
50 decomposition of analytes in the liner. Thus, the glass liner was deactivated before isotope  
51 measurement. For deactivation, BSTFA (*N, O*-bis (trimethylsilyl) trifluoroacetamide, SUPELCO)  
52 was injected manually into the GC inlet (The Agilent multimode inlet). The detailed steps are as  
53 below: temperature of the GC injector was adjusted to 100 °C, constant flow was adjusted to 1  
54 mL min<sup>-1</sup> and the split ratio was set to 200:1; The gas flow of the gas chromatography-mass  
55 spectrometry (GC-IRMS) system was set to backflush-on mode to protect the combustion unit; 1  
56  $\mu\text{L}$  of BSTFA was injected manually for 3 time waiting for 4 to 5 min between the injections.  
57 After 20 min, the temperature of injector was adjusted to 180 °C and the GC oven was heated up  
58 to 280 °C for 30 min for removing the residues from the column.

### 59 **S2.2. Extraction and clean-up of OPs for analysis**

60 The DCM extracts (see section 2.4) were purified prior gas chromatographic separation before  
61 analysis for concentration and isotope composition. For cleanup of the residue OPs and the  
62 metabolites after reaction, column chromatography was used. The anhydrous  $\text{Na}_2\text{SO}_4$  for drying  
63 the extracts were activated by heating at 200 °C overnight and stored in an airtight container.  
64 Florisil<sup>®</sup> for column chromatography was activated at 120 °C for 12 h before use.  
65 The chromatographic column (20 mm ID \* 20 cm) was filled from the bottom to the top with 0.5  
66 cm glass wool, 1 cm cleaned sea sand as a filter, 12 cm activated Florisil<sup>®</sup> and 4 cm activated

67 anhydrous Na<sub>2</sub>SO<sub>4</sub>. The column was pre-eluted with 15 ml DCM and the eluate was disposed.  
68 Then the extract was added on the top of the column and eluate was collected into a 20 ml glass  
69 vial. 15 mL DCM was added to elute the OPs and metabolites through the column with a natural  
70 flow rate. The eluate was collected into another 20 ml glass vial. The eluates were combined in a  
71 200 ml evaporation tube and the DCM was reduced by an evaporator (TurboVap II, Biotage AB,  
72 Sweden) with a gentle N<sub>2</sub> stream at room temperature to 2 mL. The recovery of this method was  
73 found to be better than 80% when material from a control experiment spiked with Parathion was  
74 extracted. Aliquots of the extract were used for concentration and isotope analysis.

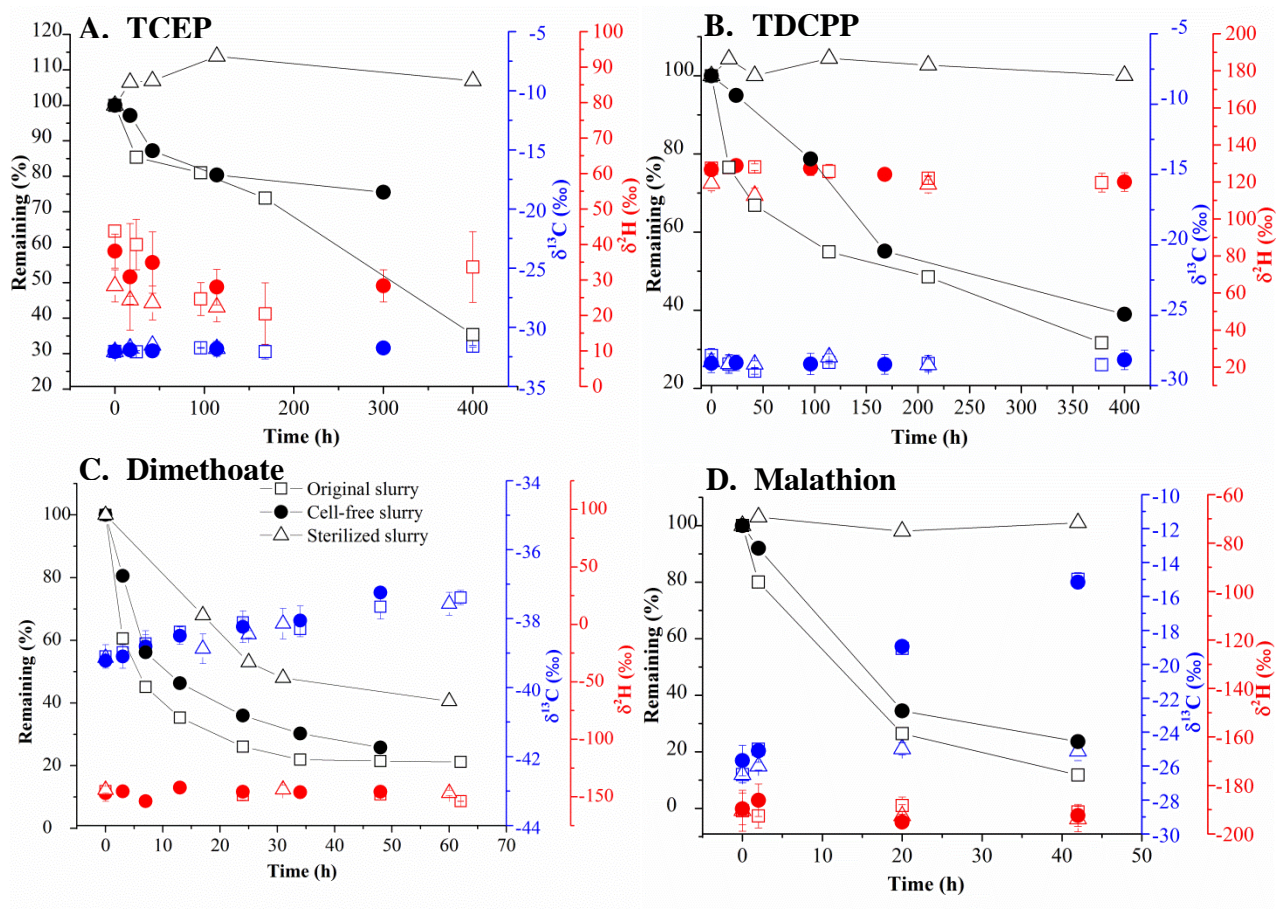
### 75 **S3. Biotransformation of OPs**

#### 76 **S3.1. Transformation of OPs in biogas slurry**

77 TCEP, TDCPP, Parathion, Parathion-methyl, Dimethoate and Malathion can be transformed in  
78 anaerobic digestion (AD) system. The transformation process of these OPs can be characterized  
79 by the first-order kinetic (**Fig. S2**), which allows to assess the isotope fractionation with the  
80 Rayleigh concept employing compound-specific stable isotope analysis (CSIA).  
81 The rate constants for degradation of TCEP and TDCPP in original slurry and cell-free slurry  
82 after 25-fold dilution were described in **Section 1.1**. The sterilized control experiments showed no  
83 degradation during period of almost 400 h. Carbon isotope compositions ranged from  $-32.0 \pm 0.1\text{‰}$   
84 to  $-31.6 \pm 0.1\text{‰}$  and from  $-27.8 \pm 0.5\text{‰}$  to  $-28.5 \pm 0.4\text{‰}$  for TCEP and TDCPP in original slurry,  
85 respectively. Similar trends were found in cell-free slurry. Values of  $\delta^{13}\text{C}$  varied from  $-32.1 \pm 0.1\text{‰}$   
86 to  $-31.8 \pm 0.3\text{‰}$  in TCEP and from  $-28.4 \pm 0.6\text{‰}$  to  $-28.2 \pm 0.7\text{‰}$  in TDCPP. The hydrogen  
87 isotope compositions of TCEP (from  $44 \pm 2\text{‰}$  to  $34 \pm 5\text{‰}$  in original slurry, from  $38 \pm 5\text{‰}$  to  $28$   
88  $\pm 5\text{‰}$  in cell-free slurry) and TDCPP (from  $127 \pm 3\text{‰}$  to  $120 \pm 5\text{‰}$  in original slurry, from  $127 \pm$   
89  $1\text{‰}$  to  $120 \pm 5\text{‰}$  in cell-free slurry) were almost constant. Hence, neither significant carbon nor

90 hydrogen fractionations could be detected.

91 In original slurry diluted with five fold, the degradation rates of  $39.6 \pm 7.9 \times 10^{-3} \text{ h}^{-1}$  and  $50.5 \pm$   
92  $5.3 \times 10^{-3} \text{ h}^{-1}$  were estimated for Dimethoate and Malathion, respectively. Dimethoate was  
93 degraded (ca. 60%) in sterilized slurry with the rate constant of  $14.8 \pm 3.5 \times 10^{-3} \text{ h}^{-1}$ , and it is  
94 consistent with the rate constants of abiotic hydrolysis, which are about  $18.4 \times 10^{-3} \text{ h}^{-1}$  at pH 7  
95 and  $12.3 \times 10^{-3} \text{ h}^{-1}$  at pH 9 (Wu et al., 2018), indicating hydrolysis took place at pH 7.4. Whereas,  
96 the sterilized control experiments showed no degradation within 50 h for Malathion. The carbon  
97 isotope compositions of Dimethoate and Malathion were described in **Section 1.2**. The hydrogen  
98 isotope compositions of Dimethoate and Malathion ranged from  $-145 \pm 3\text{‰}$  to  $-153 \pm 1\text{‰}$  and  
99 from  $-190 \pm 8\text{‰}$  to  $-191 \pm 1\text{‰}$  in original slurry, respectively (**Fig. S1**). In the cell-free slurry,  
100 values of Dimethoate ranged from  $-147 \pm 7\text{‰}$  to  $-146 \pm 4\text{‰}$  and from  $-190 \pm 7\text{‰}$  to  $-192 \pm 5\text{‰}$   
101 in experiments with Malathion.



102

103 **Fig. S1.** The concentrations (black symbols) and stable isotope compositions of TCEP (A),

104 TDCPP (B), Dimethoate (C) and Malathion (D) during biotransformation in the biogas slurry.

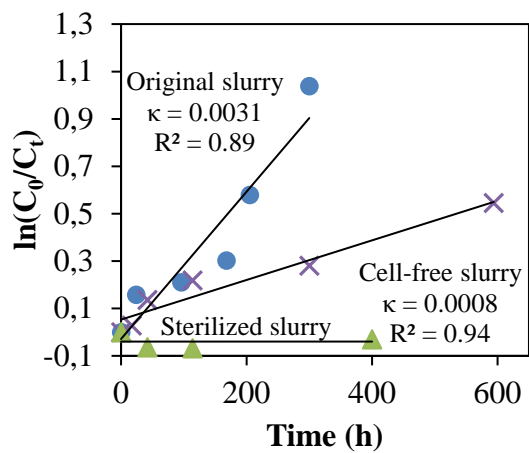
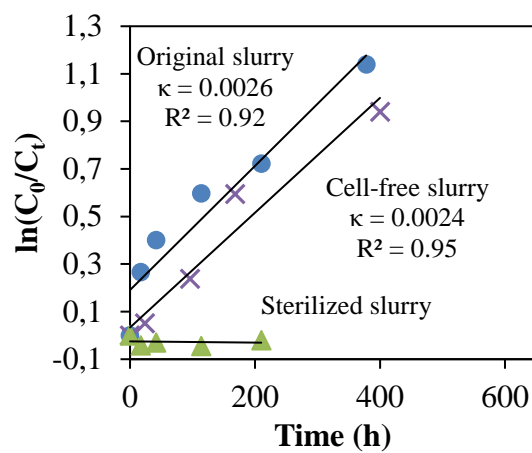
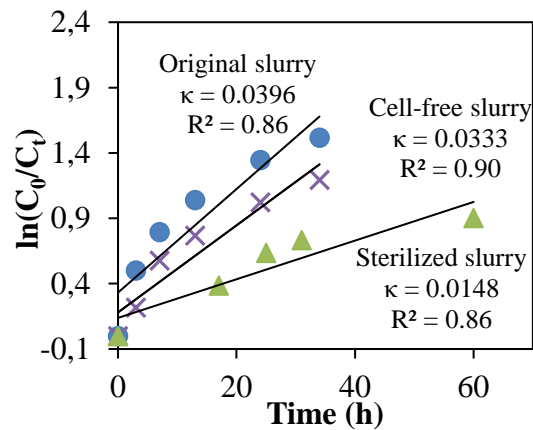
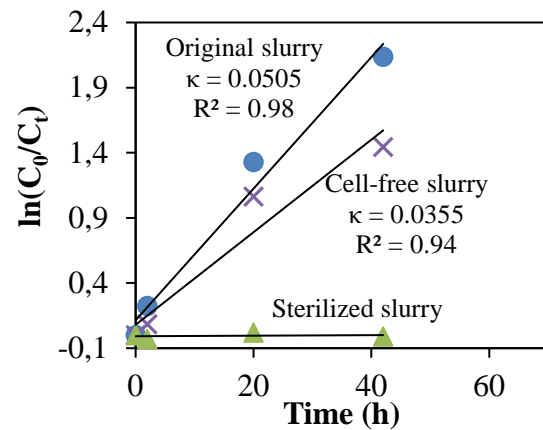
105 Carbon and hydrogen isotope compositions are represented by blue and red symbols.

106 Experiments with original slurry, cell-free slurry and sterilized slurry are represented by empty

107 square (□), dark circle (●) and empty triangle (△).

108

109

**A. TCEP****B. TDCPP****C. Dimethoate****D. Malathion**

110

111 **Fig. S2.** The first-order kinetics of TCEP (A), TDCPP (B), Dimethoate (C) and Malathion (D)

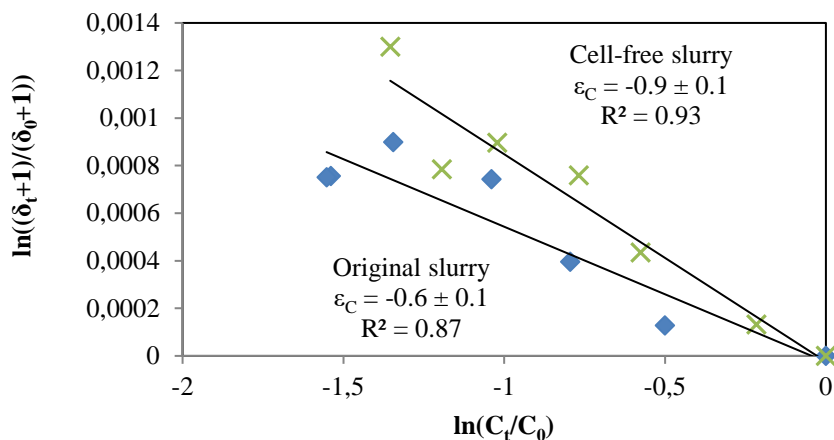
112 upon biodegradation in original biogas slurry. Experiments with original slurry, cell-free slurry

113 and sterilized slurry are represented by ●, × and ▲, respectively.

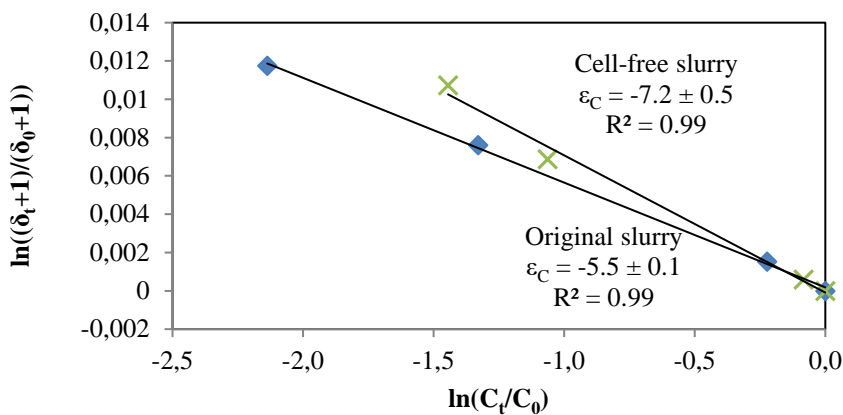
114

115

**A. Dimethoate**



**B. Malathion**

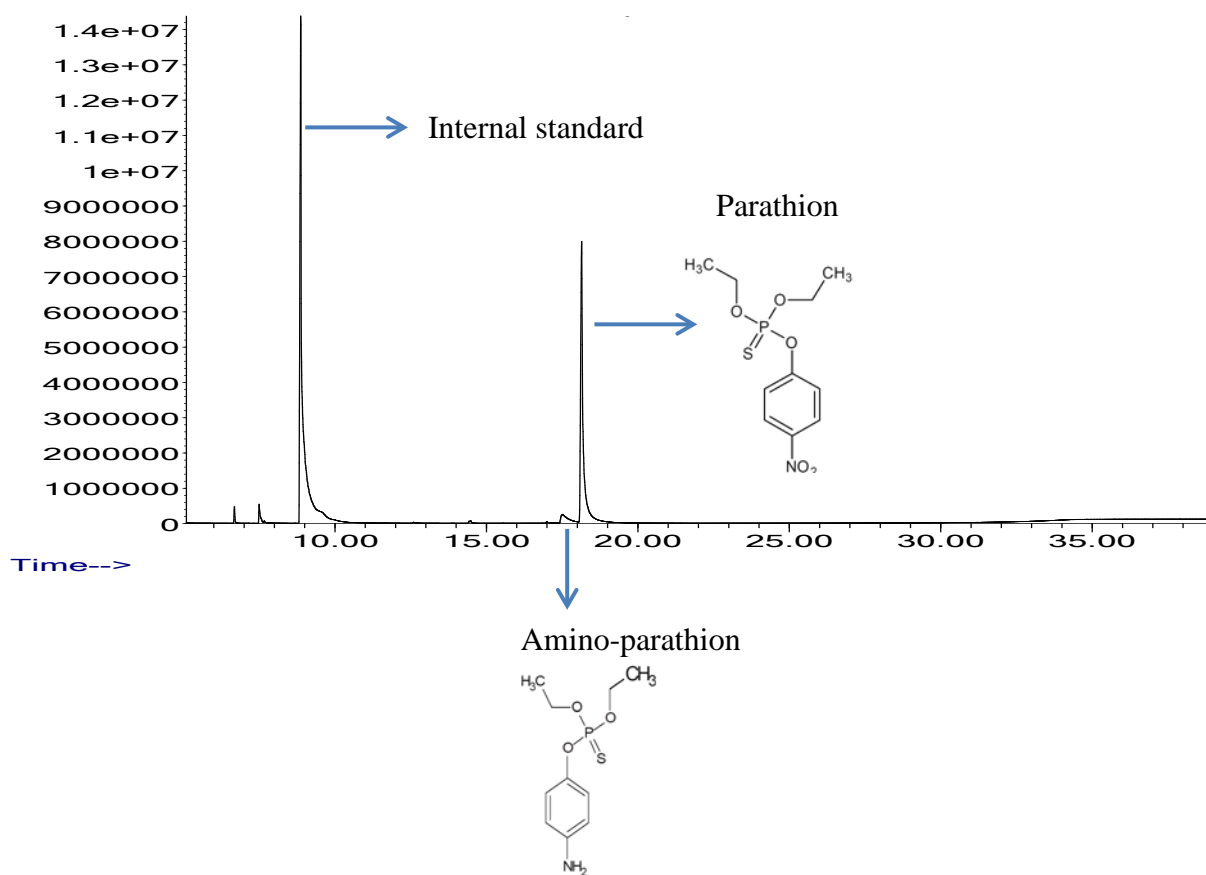


117

118 **Fig. S3.** The Rayleigh plots of carbon isotope fractionations of Dimethoate and Malathion during  
 119 transformation in biogas slurry. Experiments with original slurry and cell-free slurry are  
 120 represented by  $\blacklozenge$  and  $\times$ , respectively.

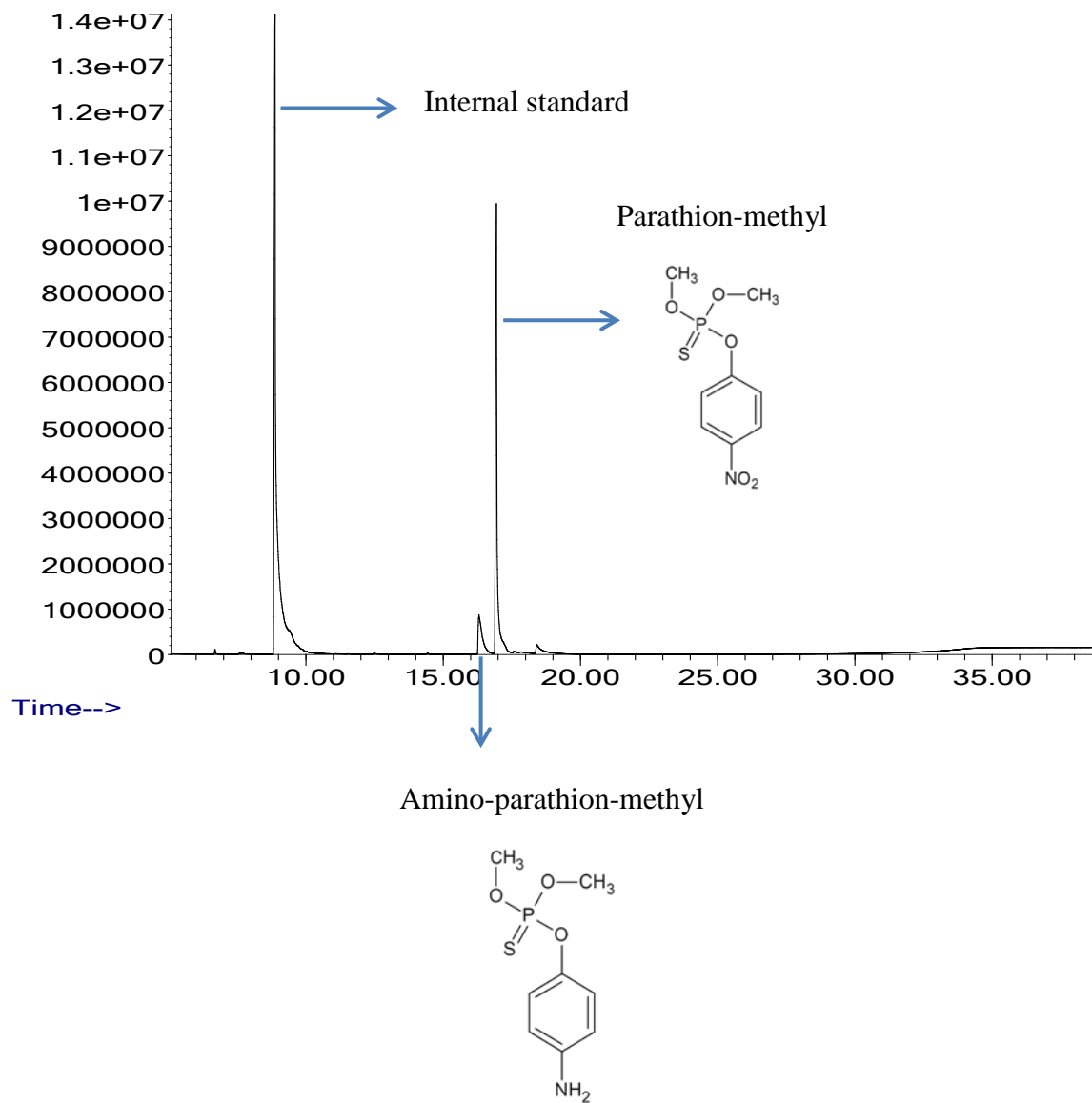
121 **S4. Identification of metabolites by GC-MS**

122 The GC amenable metabolites were analyzed and identified by GC-MS. At the beginning of the  
123 experiment (time = 0 min) only the parent compounds with internal standards were observed. In  
124 samples after degradation to a certain extent reported in % of initial concentration metabolites  
125 described below show transformation of OPs in AD (**Fig. S4-S7**).



126

127 **Fig. S4.** Metabolites of Parathion analyzed by GC-MS found in the system after 3h (ca. 30%  
128 degradation). Parathion was added to 50-fold dilution of original biogas slurry. Amino-parathion  
129 was detected by the mass spectra.

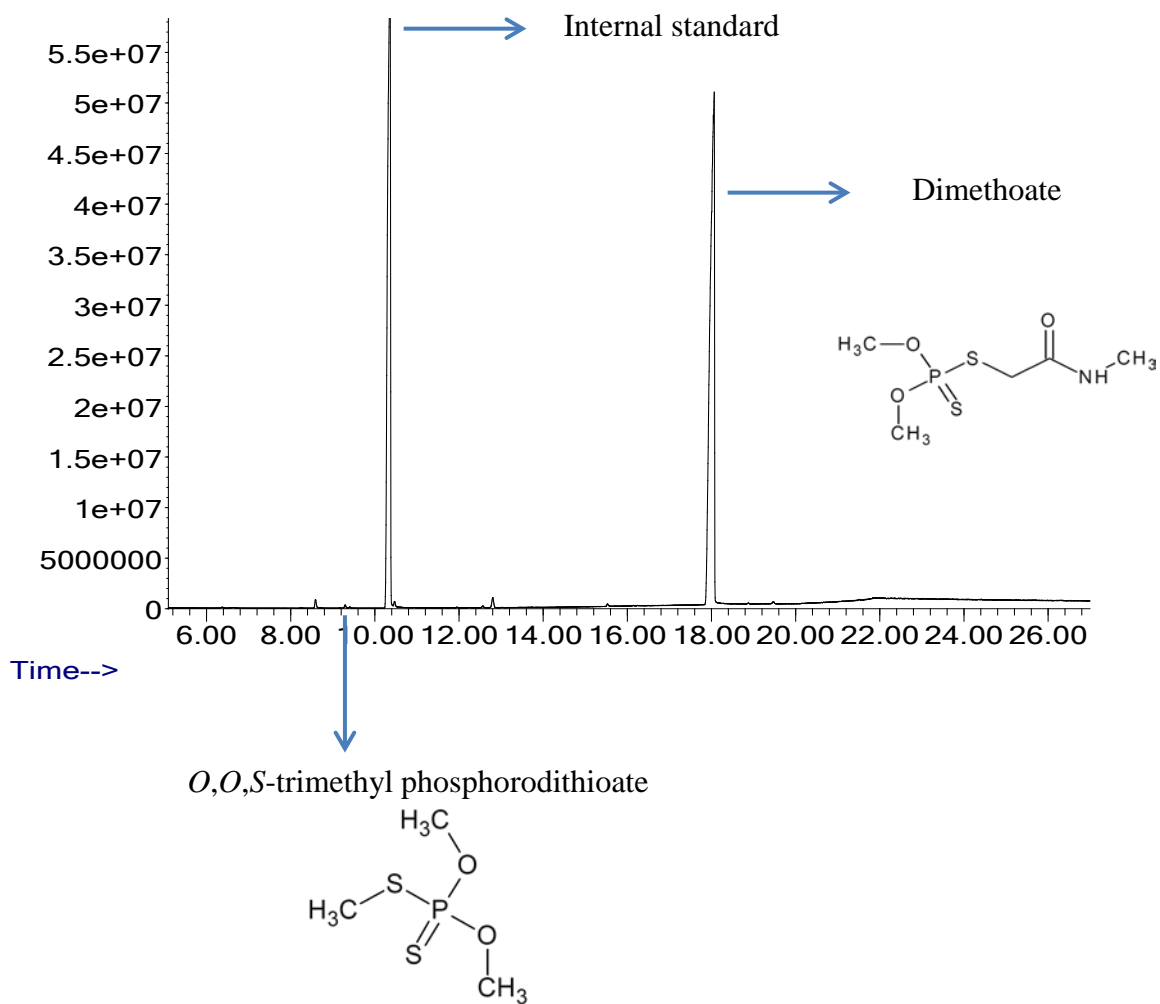


130

131 **Fig. S5.** Metabolites of Parathion-methyl analyzed by GC-MS after 21h (ca. 40% degradation).

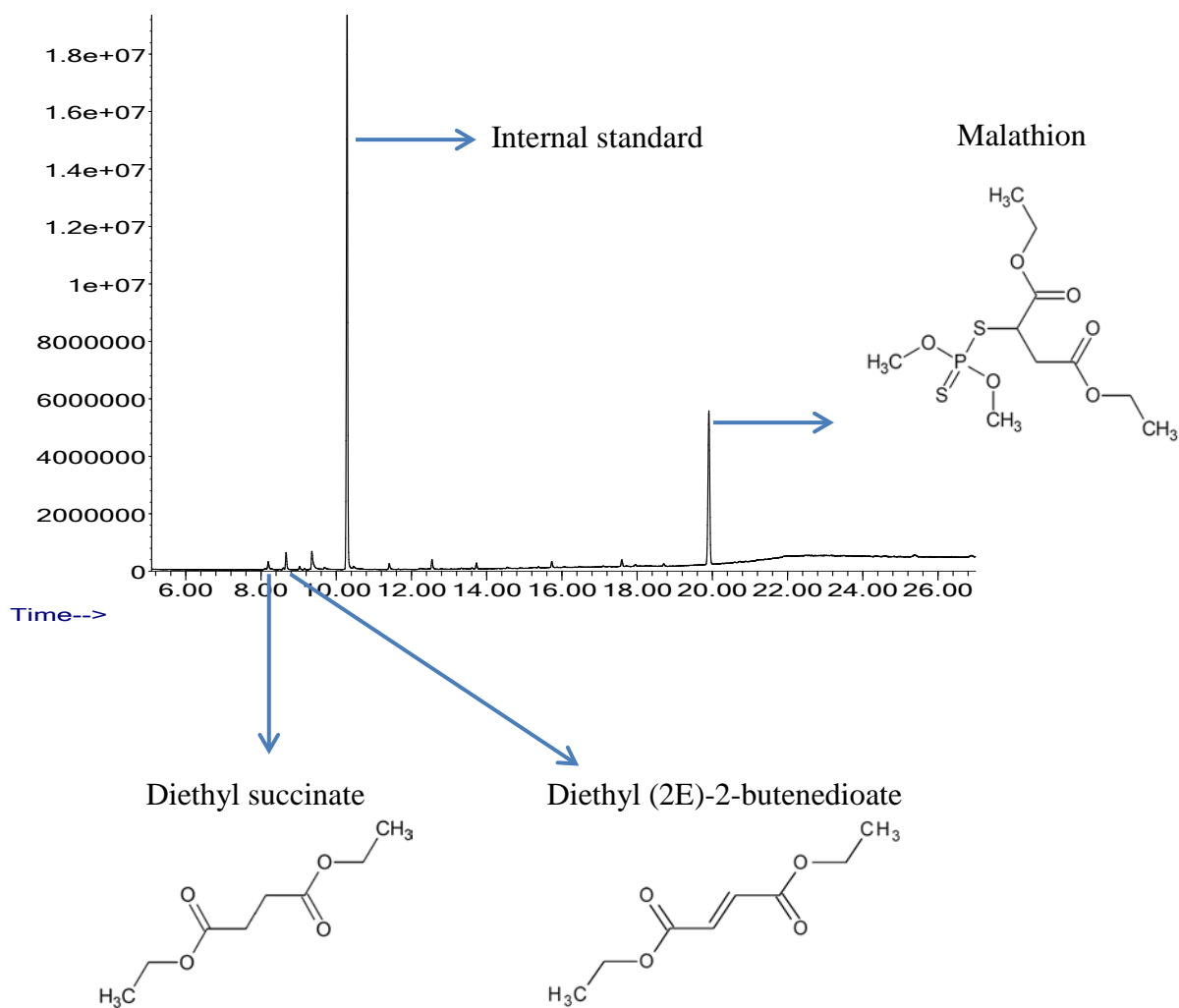
132 Amino-parathion-methyl was detected as metabolite.

133



135

136 **Fig. S6.** Metabolites of Dimethoate analyzed by GC-MS. *O,O,S*-trimethyl phosphorodithioate  
 137 was tentatively identified by the mass spectrum after 62 h (ca. 70% degradation). Dimethoate  
 138 was added to 5-fold dilution of original biogas slurry.



140 **Fig. S7.** Metabolites of Malathion were tentatively identified by their mass spectra using GC-MS.

141 Malathion was added to 5-fold dilution of original biogas slurry and the compounds were

142 detected in the system after 20 h (ca. 70% degradation). Diethyl succinate and diethyl (2E)-2-

143 butenedioate were identified.

144

## 145 **S5. Characterization of metabolites by FT-ICR MS**

### 146 **S5.1. Preparation of samples**

147 Three sets of samples were prepared for the analysis of metabolites: one set was prepared in tris-  
148 HCl buffer rather than biogas slurry as control set (OP-C), and it was stopped at 0 hour point  
149 with 6 N HCl as described in **section 2.4**; another two sets of experiments were conducted with  
150 biogas slurry and were stopped at hour **0** (OP-0) and hour **t** after achieving ~ 50% degradation  
151 (OP-t, specific t-time points are described in each section for each OP below). The experiments  
152 were conducted at 37 °C. For solid phase extraction (SPE), 10 mL of aqueous solution was  
153 extracted with 100 mg Bond Elut PPL cartridges (Agilent) for analysis of metabolites.

154 The SPE procedures were as followed: cleaning with 1 mL methanol; conditioning the cartridges  
155 with 2 mL acidic water (pH 2 adjusted with HCl); loading 10 mL of aqueous sample which was  
156 adjusted to pH 2 using HCl; drying the cartridge with vacuum pump; washing with 1 mL acidic  
157 water to remove the residual buffer salts; totally drying the cartridges with vacuum pump and  
158 elution of the transformation products with 1 mL methanol. The methanolic extract was collected  
159 and diluted 1:100 (v/v) with MilliQ water /MeOH mixture (1:1, v/v) before analysis.

160 A Fourier-transform ion cyclotron resonance mass spectrometer (FT-ICR MS, Solarix XR 12T,  
161 Bruker Daltonics) equipped with a dynamically harmonized analyzer cell was used for the  
162 analysis of methanolic extracts. Samples were measured with positive and negative modes of  
163 electrospray ionization (ESI) in direct infusion mode with a 4 MWord time domain using typical  
164 ESI conditions. MeOH/MQW 1:1 was used as solvent. For each spectrum 128-256 scans were  
165 co-added with an ion accumulation time of 50 ms for positive mode and 350 ms for negative

166 mode, respectively. The instrument was calibrated in the mass range  $m/z$  74-1000 using Arg  
167 clusters 1-4 in positive (45 ppb RMSE) and negative (71 ppb RMSE) mode (64 scans each).

168 Parts of samples were extracted as described above and were subjected to UPLC mass  
169 spectrometric analysis using a Q-ToF system (Waters Synapt) to confirm the relative abundances  
170 of the compounds. In this case the compounds were separated by UPLC before ESI was used in  
171 positive mode for detection.

## 172 **S5.2. Identified metabolites**

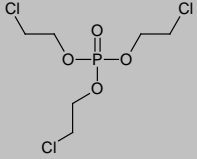
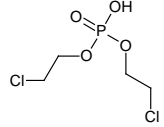
173 Extracted samples from transformation experiments were analyzed by FT-ICR MS using positive  
174 and negative modes of electrospray ionization. The masses detected in positive or negative mode  
175 are summarized in tables for each OP compound. All the listed metabolites are detectable via FT-  
176 ICR MS. The abundance (with 1 ppm mass error) and intensities of mass fragments at time 0  
177 (OP-0) and after compound specific degradation time (OP-t) were compared in order to analyze  
178 the formation of metabolites. In few cases, especially where hydrolysis can take place, potential  
179 metabolites were already present in the OP-0 samples, indicating a very fast reaction in the slurry.  
180 Only the monoisotopic peaks were considered for analysis.

### 181 **S5.2.1. TCEP (tris(2-chloroethyl) phosphate)**

182 Sample incubated with biogas slurry was sacrificed at 280h and all samples were measured in  
183 positive mode only (**Table S2**).

#### 184 **Table S2. Proposed metabolites of TCEP**

#	Name	Formula	structure	$[M+H]^+$	<i>m/z</i> detected (intensity, mono)
---	------	---------	-----------	-----------	------------------------------------------

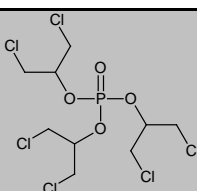
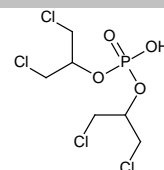
Parent compound	TCEP	C <sub>6</sub> H <sub>12</sub> Cl <sub>3</sub> O <sub>4</sub> P		284.9612 (mono) 286.9583 ( <sup>37</sup> Cl <sub>1</sub> )	pos: OP-C: 0.96×10 <sup>9</sup> OP-0: 5.65×10 <sup>9</sup> OP-t: 3.13×10 <sup>9</sup>
1	bis(2-chloroethyl) hydrogen phosphate	C <sub>4</sub> H <sub>9</sub> Cl <sub>2</sub> O <sub>4</sub> P		222.9688 (mono)	pos: OP-C: n.d. OP-0: 1.86×10 <sup>7</sup> OP-t: 1.04×10 <sup>7</sup>
1* (sodium adduct)				244.9507 [M+Na <sup>+</sup> ] <sup>+</sup>	pos: OP-C: 0.86×10 <sup>7</sup> OP-0: 0.92×10 <sup>7</sup> OP-t: 1.19×10 <sup>7</sup>

185 pos: positive mode. n.d.: not detected.

### 186 S5.2.2. TDCPP (tris(1,3-dichloro-2-propyl) phosphate)

187 Sample incubated with biogas slurry was sacrificed at 114h and all samples were measured in  
188 positive mode only (**Table S3**).

189 **Table S3. Proposed metabolites of TDCPP**

#	Name	Formula	structure	[M+H <sup>+</sup> ] <sup>+</sup>	<i>m/z</i> detected (intensity, mono)
Parent compound	TDCPP	C <sub>9</sub> H <sub>15</sub> Cl <sub>6</sub> O <sub>4</sub> P		428.8912 (mono) 430.8883 ( <sup>37</sup> Cl <sub>1</sub> )	pos: OP-C: 4.17×10 <sup>7</sup> OP-0: 4.58×10 <sup>7</sup> OP-t: 3.41×10 <sup>7</sup>
1	bis(1,3-dichloro-2-propyl) hydrogen phosphate	C <sub>6</sub> H <sub>11</sub> Cl <sub>4</sub> O <sub>4</sub> P		318.9221 (mono)	pos: OP-C: 1.54×10 <sup>6</sup> OP-0: 0.4×10 <sup>7</sup> OP-t: 1.2×10 <sup>7</sup>

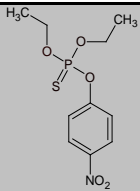
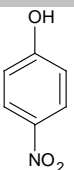
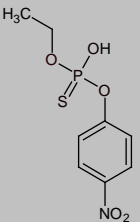
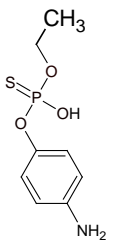
190 pos: positive mode.

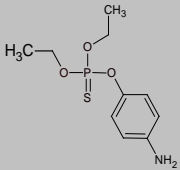
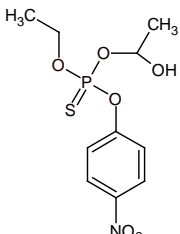
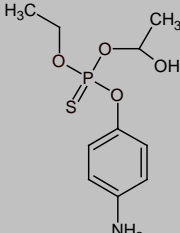
191

192 **S5.2.3. Parathion (O,O-diethyl-O-(4-nitrophenyl) phosphorothioate)**

193 The detected metabolites of the FT-ICR MS are summarized in **Table S4** and the intensity of  
 194 OP-t in the table is from incubated samples of 288h. To confirm the results of FT-ICR MS, the  
 195 metabolites formed during degradation of Parathion in the slurry were analyzed using UPLC-Q-  
 196 ToF-MS. Amino-parathion, O-ethyl O-(4-nitrophenyl)phosphorothionate, p-nitrophenol, O-ethyl  
 197 O-(4-aminophenyl)phosphorothioate were confirmed by their mass spectra.

198 **Table S4. Proposed metabolites of Parathion**

#	Name	Formula	structure	[M+H] <sup>+</sup>	[M-H] <sup>-</sup>	m/z detected (intensity)
Parent compound	Parathion	C <sub>10</sub> H <sub>14</sub> NO <sub>5</sub> PS		292.0403	290.0258	pos: OP-C: 3.64×10 <sup>8</sup> OP-0: 2.04×10 <sup>9</sup> OP-t: 4.56×10 <sup>9</sup> neg: OP-C: 1.55×10 <sup>8</sup> OP-0: 1.55×10 <sup>8</sup> OP-t: 1.73×10 <sup>8</sup>
1	<i>p</i> -nitrophenol	C <sub>6</sub> H <sub>5</sub> NO <sub>3</sub>		140.0342	138.0197	neg: OP-C: 0.26×10 <sup>9</sup> OP-0: 0.56×10 <sup>9</sup> OP-t: 1.09×10 <sup>9</sup>
2	<i>O</i> -ethyl <i>O</i> -(4-nitrophenyl) phosphorothioate	C <sub>8</sub> H <sub>10</sub> NO <sub>5</sub> PS		264.0090	261.9945	neg: OP-C: 1.76×10 <sup>10</sup> OP-0: 2.21×10 <sup>10</sup> OP-t: 3.33×10 <sup>10</sup>
3	<i>O</i> -ethyl <i>O</i> -(4-aminophenyl) phosphorothioate	C <sub>8</sub> H <sub>12</sub> NO <sub>3</sub> PS		234.0348	232.0203	pos: in EP-t incubated samples OP-C: n.d. OP-0: n.d. OP-t: 8.28×10 <sup>7</sup> <b>(Fig. S9-S11)</b>

4	amino-parathion	$C_{10}H_{16}NO_3PS$		262.0661	260.0516	pos: in EP-t incubated samples OP-C: n.d. OP-0: n.d. OP-t: $3.81 \times 10^9$ <b>(Fig. S8)</b>
5	<i>O</i> -ethyl <i>O</i> -(1,1-ethanediyl) <i>O</i> -(4-nitrophenyl) phosphorothioate	$C_{10}H_{14}NO_6PS$		308.0352	306.0207	neg: in EP-0 and incubated samples <b>(Fig. S12)</b> OP-C: n.d. OP-0: $6.77 \times 10^7$ OP-t: $7.36 \times 10^7$
6	<i>O</i> -ethyl <i>O</i> -(1,1-ethanediyl) <i>O</i> -(4-aminophenyl) phosphorothioate	$C_{10}H_{16}NO_4PS$		278.0610	276.0465	neg: in EP-0 and incubated samples <b>(Fig. S13)</b> OP-C: n.d. OP-0: $1.37 \times 10^8$ OP-t: $1.40 \times 10^8$

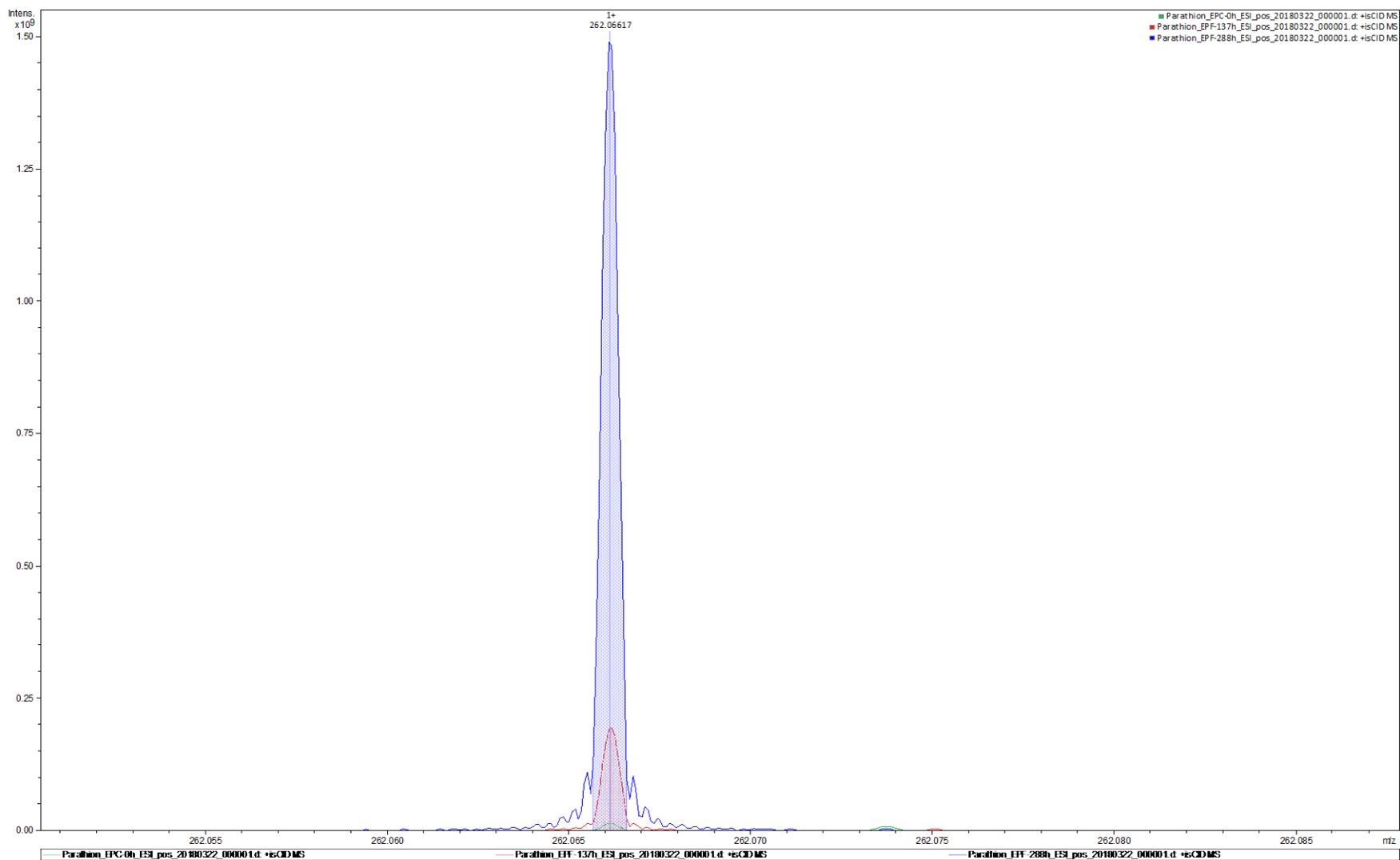
199 neg: negative mode; pos: positive mode; n.d.: not detected.

200

201 In positive mode, peak of Parathion could be detected in EP-C, EP-0 and EP-t. Peaks of amino-

202 parathion at  $m/z$  262.0661 were only detected in the incubated samples EP-t.

203



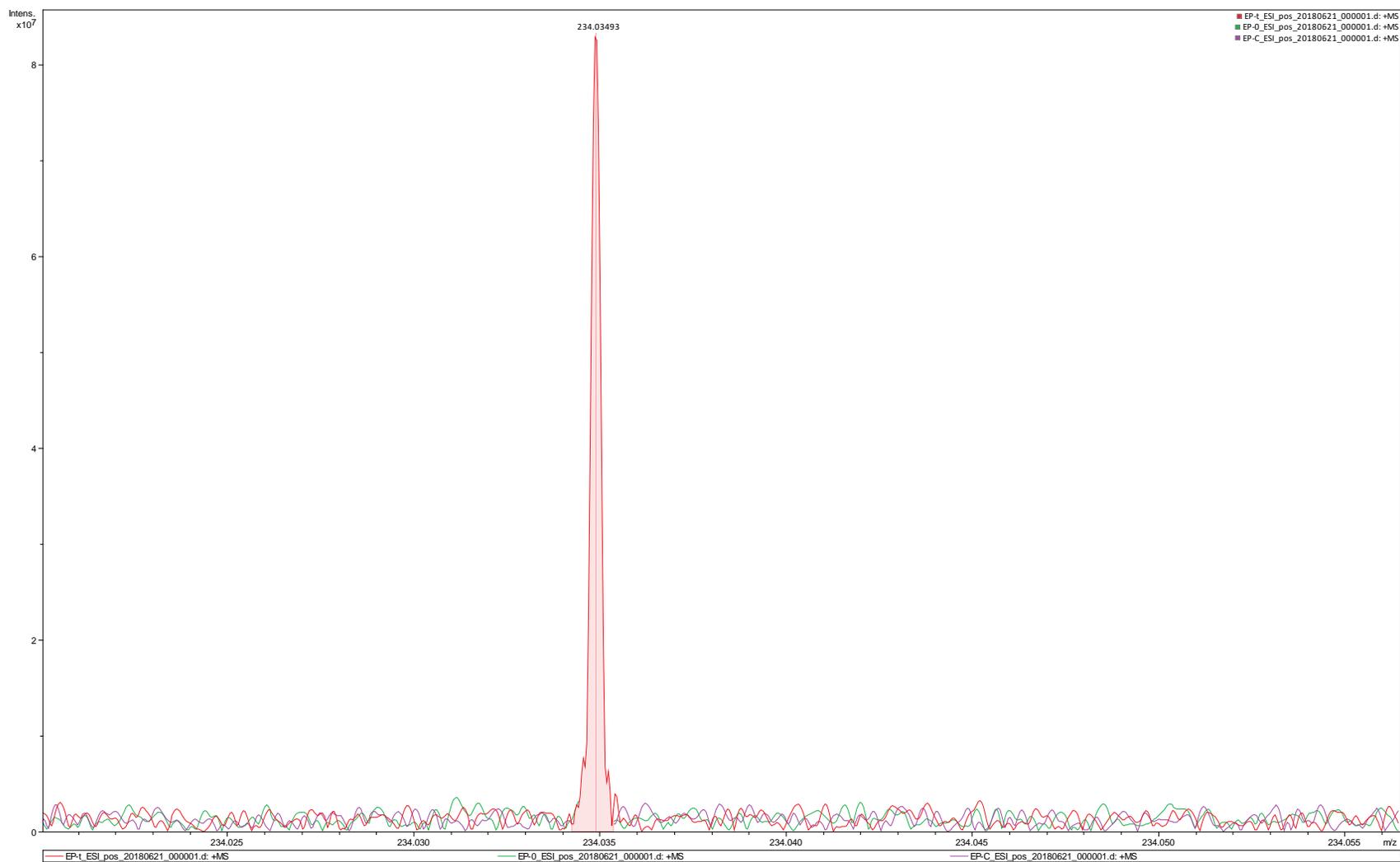
204

205 **Fig. S8.**  $[M+H]^+$  peaks of amino-parathion at  $m/z$  262.0661 in EP-C (green), EP-t<sub>137h</sub> (red) and EP-t<sub>288h</sub> (blue).

206 Moreover, a peak corresponding to the mass of protonated *O*-ethyl *O*-(4-aminophenyl)-  
207 phosphorothioate ( $m/z = 234.0348$ ) could be detected in the EP-t samples, but it was absent in  
208 EP-C and EP-0 samples.

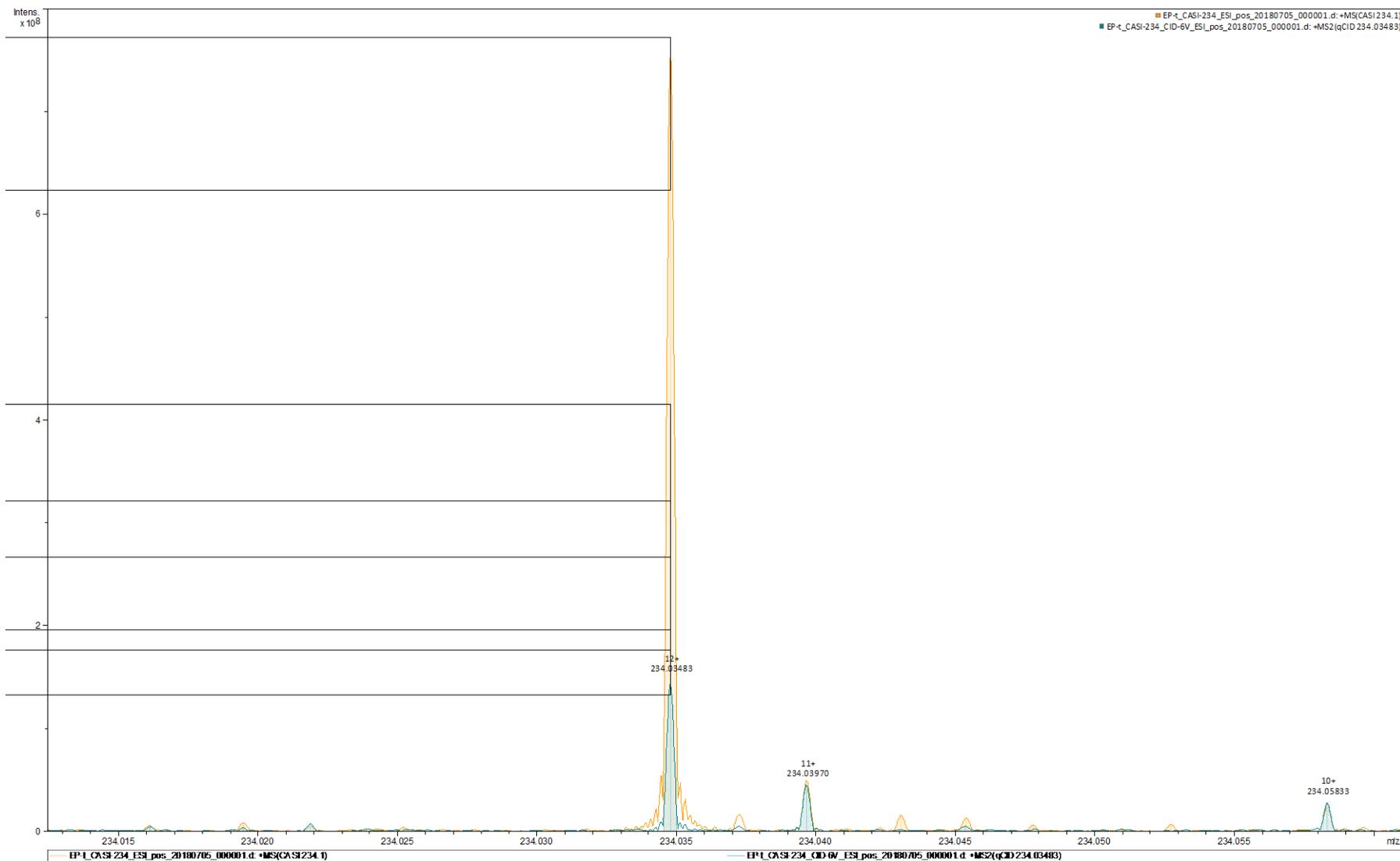
209 The peak was isolated using the Q1 (continuous accumulation of selected ions, CASI), and  
210 isolation window was set to 1.5 Da. Furthermore, collision-induced dissociation (CID) was  
211 performed with the collision voltage set to 6V. During CID experiment, a fragment at  $m/z$  110.06  
212 could be detected, which corresponds to the mass of an aminophenyl-cation. This peak could not  
213 be observed in the standard CASI-spectrum. Hence, the peak with the mass  $m/z$  234.0348 was  
214 identified as *O*-ethyl *O*-(4-aminophenyl)-phosphorothioate. Moreover, deduced from the absence  
215 of such a peak in the control and  $t_0$ -samples, the formation of *O*-ethyl *O*-(4-aminophenyl)-  
216 phosphorothioate might be due to the inoculation of biogas slurry.

217 In negative mode, appearance of peak at  $m/z$  290.0258 (Parathion) could be detected in all  
218 samples. Furthermore, peaks representing nitrophenol, *O*-ethyl *O*-(4-nitrophenyl)  
219 phosphorothioate, *O*-ethyl O-(1,1-ethanediyl) O-(4-nitrophenyl) phosphorothioate ( $m/z$  306.0207)  
220 and O-ethyl O-(1,1-ethanediyl) O-(4-aminophenyl) phosphorothioate ( $m/z$  276.0465) were  
221 detected in samples incubated with slurry.

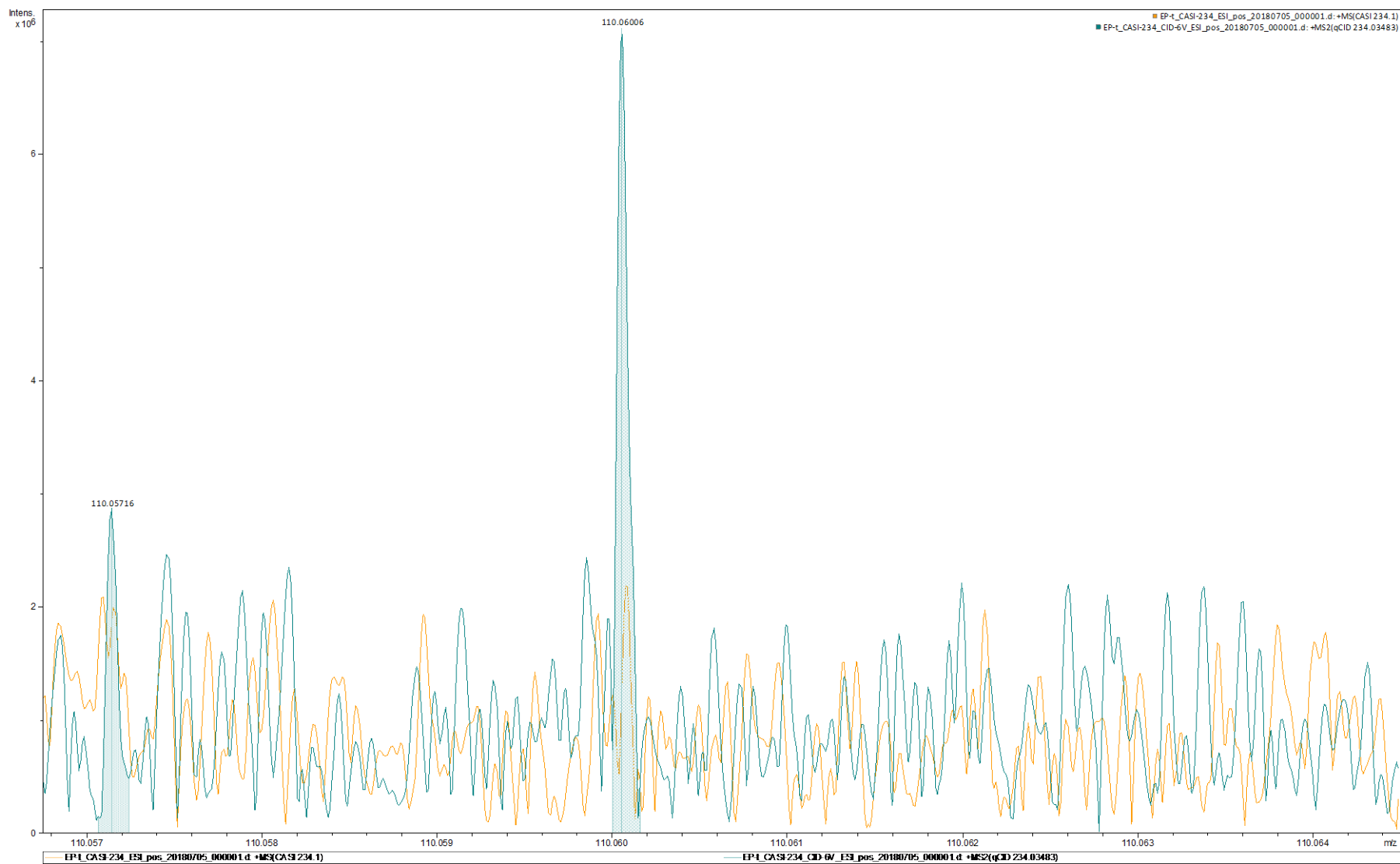


222

223 **Fig. S9.** Peaks corresponding to protonated *O*-ethyl *O*-(4-aminophenyl)-phosphorothioate at *m/z* 234.0348 (EP-C: purple, EP-0:  
224 green, EP-t: red).

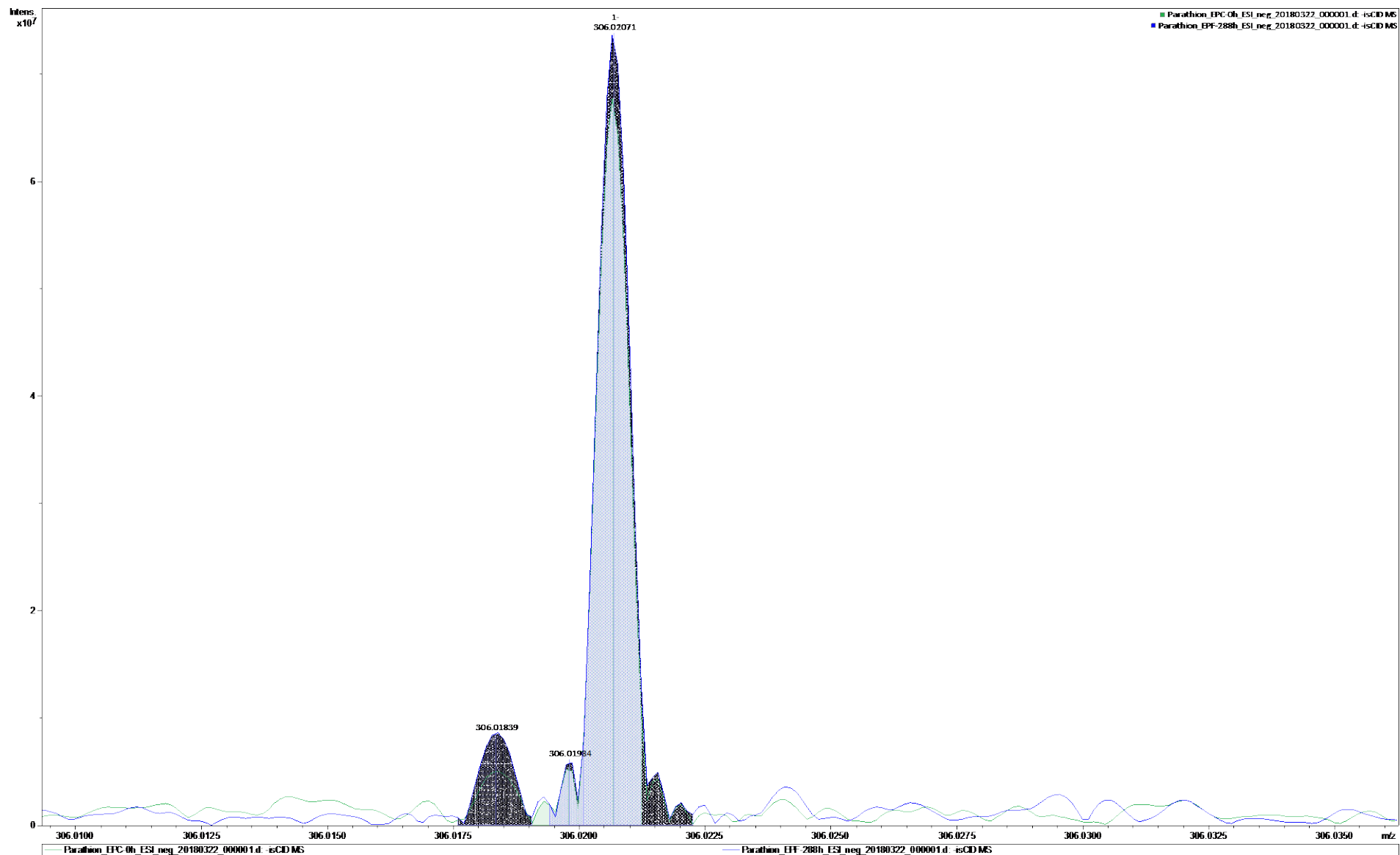


225 **Fig. S10.** Peaks corresponding to protonated *O*-ethyl *O*-(4-aminophenyl)-phosphorothioate at *m/z* 234.0348 in CASI mode. Orange:  
 226 standard CASI, green CASI-CID

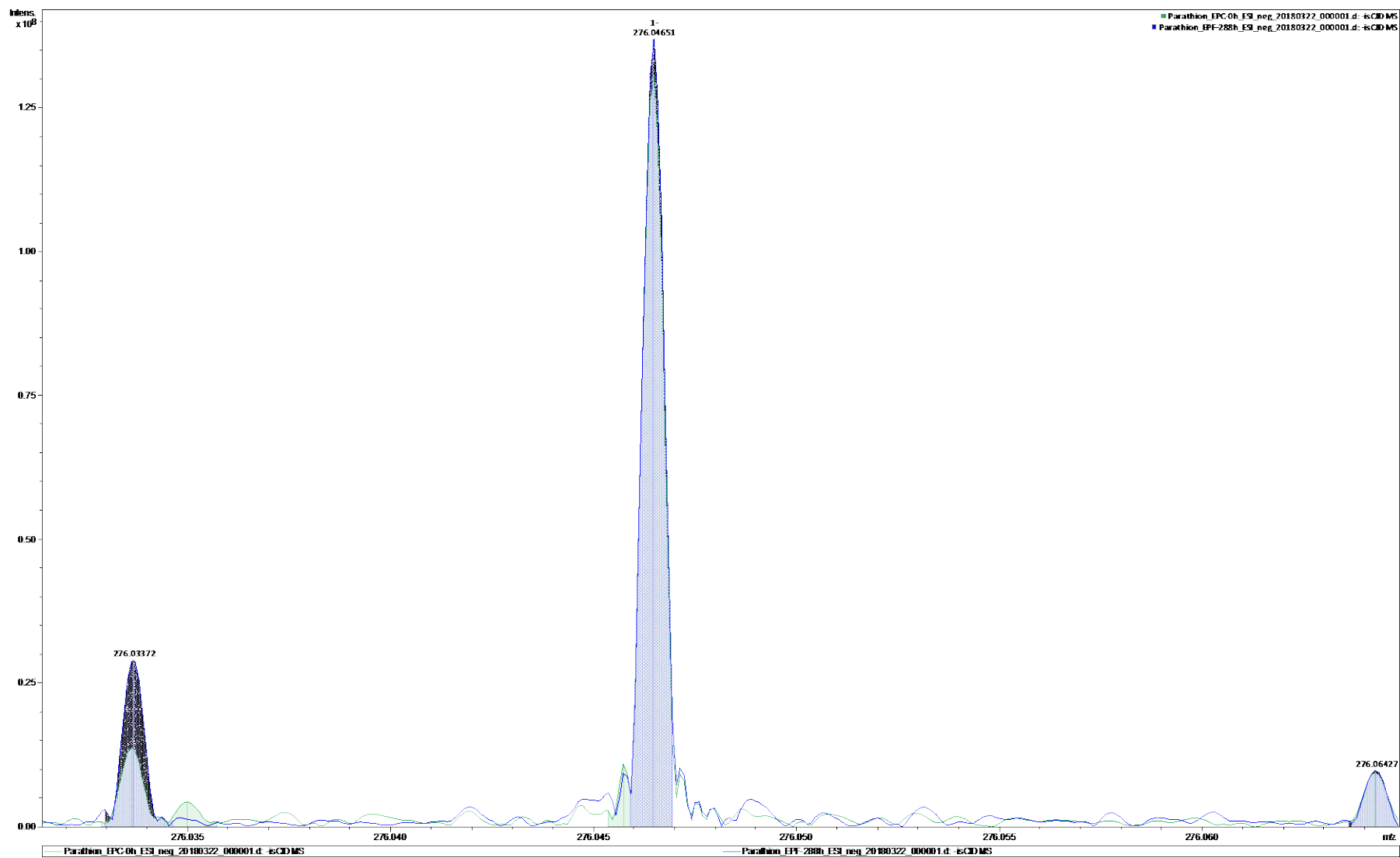


227

228 **Fig. S11.** Peak corresponding to aminophenyl-cation at  $m/z$  110.0601, present only in CID spectrum.



229 **Fig. S12.**  $[M-H]^+$  peaks of #5 ( $C_{10}H_{14}NO_6PS$ ) at  $m/z$  306.0207 in EP-0 (green) and EP-t<sub>288h</sub> (blue).



230

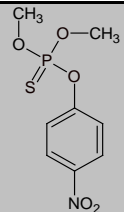
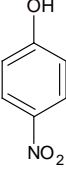
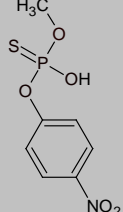
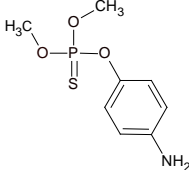
231 **Fig. S13.**  $[M-H]^+$  peaks of #6 ( $C_{10}H_{16}NO_4PS$ ) at  $m/z$  276.0465 in EP-0 (green) and EP-t<sub>288h</sub> (blue).

232 **S5.2.4. Parathion-methyl (O, O-dimethyl-O-(4-nitrophenyl) phosphorothioate)**

233 Sample incubated with biogas slurry was sacrificed at 48h and 288h for Parathion-methyl, and

234 the detected metabolites are summarized in **Table S5**.

235 **Table S5. Proposed metabolites of Parathion-methyl**

#	Name	Formula	structure	[M+H] <sup>+</sup>	[M-H] <sup>-</sup>	m/z detected (intensity)
<b>Parent compound</b>	Parathion-methyl	C <sub>8</sub> H <sub>10</sub> NO <sub>5</sub> PS		264.0090	261.9945	pos: in all samples OP-C: 1.76×10 <sup>9</sup> OP-0: 2.66×10 <sup>9</sup> OP-t: 2.49×10 <sup>9</sup> neg: in all samples OP-C: 5.96×10 <sup>7</sup> OP-0: 1.88×10 <sup>7</sup> OP-t: 0.94×10 <sup>7</sup>
<b>1</b>	<i>p</i> -nitrophenol	C <sub>6</sub> H <sub>5</sub> NO <sub>3</sub>		140.0342	138.0197	neg: OP-C: 5.99×10 <sup>9</sup> OP-0: 1.77×10 <sup>9</sup> OP-t: 2.62×10 <sup>9</sup>
<b>2</b>	<i>O</i> -methyl <i>O</i> -(4-nitrophenyl) phosphorothioate	C <sub>7</sub> H <sub>8</sub> NO <sub>5</sub> PS		249.9934	247.9788	neg: OP-C: 1.34×10 <sup>11</sup> OP-0: 0.57×10 <sup>11</sup> OP-t: 2.19×10 <sup>11</sup>
<b>3</b>	amino-parathion-methyl	C <sub>8</sub> H <sub>12</sub> NO <sub>3</sub> PS		234.0348	232.0203	pos: in MP-t sample OP-C: n.d. OP-0: n.d. OP-t: 1.19×10 <sup>9</sup> <b>(Fig. S15-S16)</b>

236 neg: negative mode; pos: positive mode; n.d.: not detected.

237 In negative mode, masses representing Parathion-methyl (m/z 261.9945) were detected in all

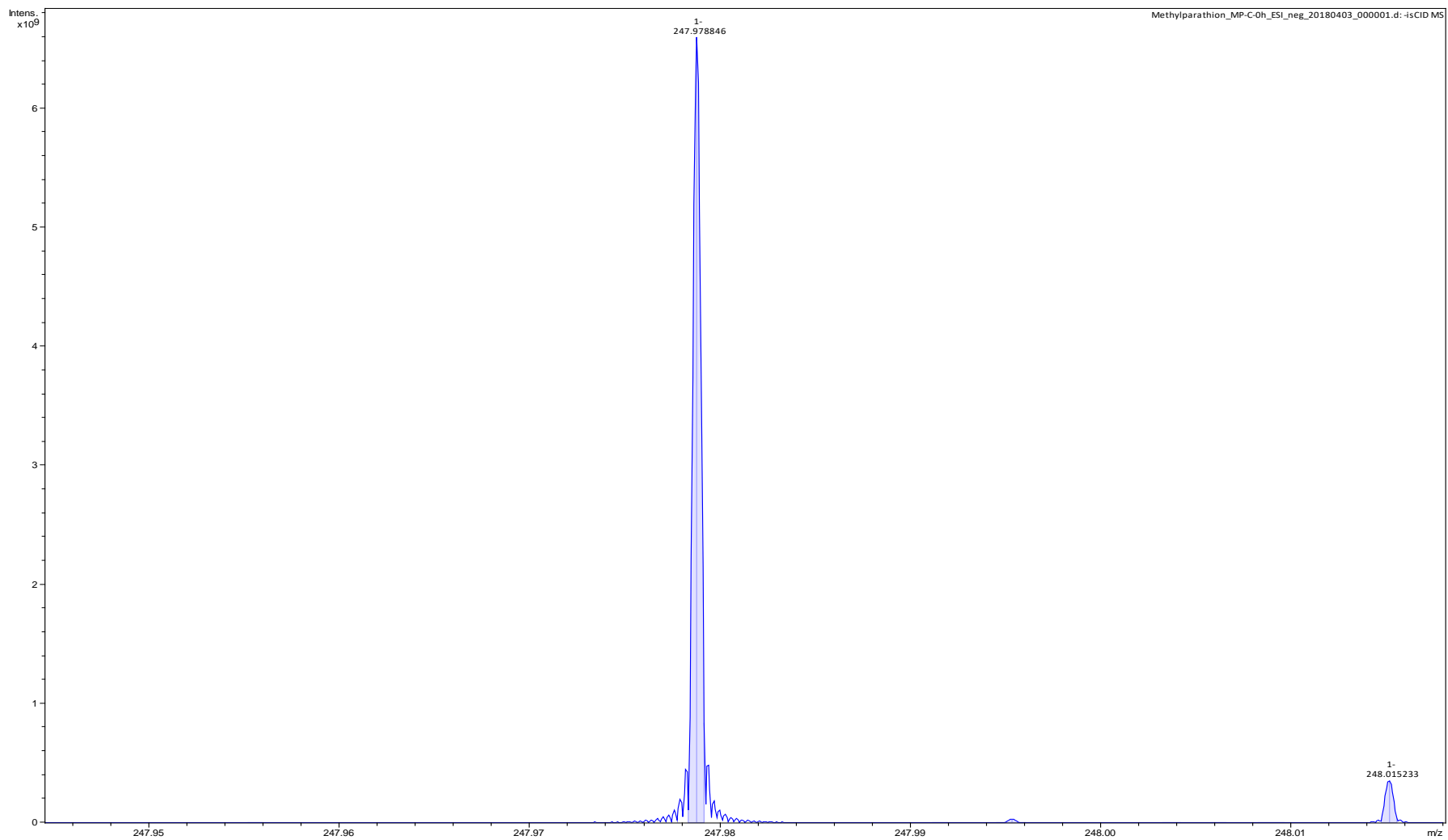
238 samples. Masses of *O*-methyl *O*-(4-nitrophenyl) phosphorothioate (m/z 247.9788) and

239 nitrophenol at m/z 138.0197 were found in all samples. However, the abundance in MP- t<sub>288h</sub> are  
240 relatively higher than MP-C.

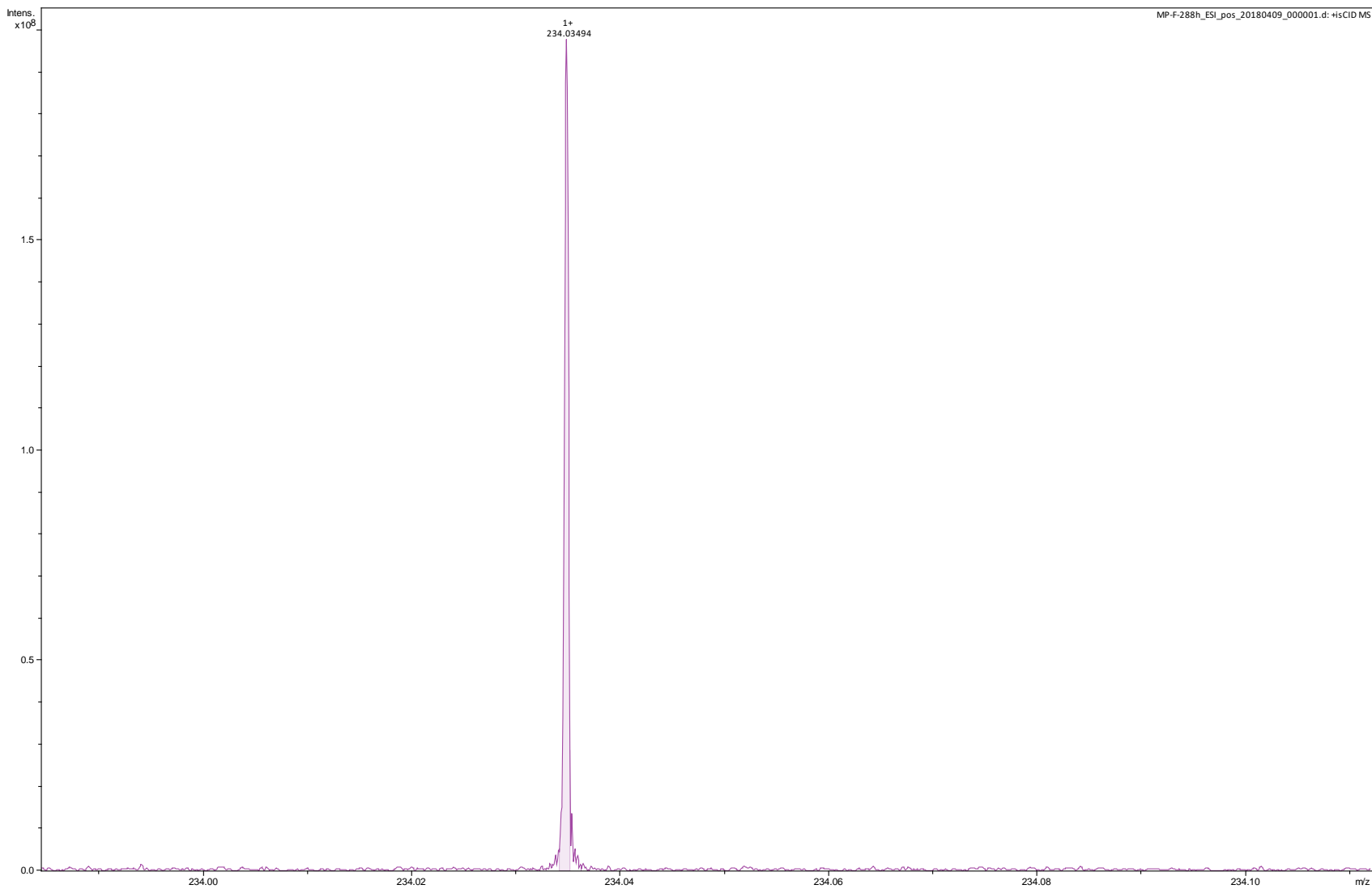
241 In MP-C, peak of *O*-methyl *O*-(4-nitrophenyl) phosphorothioate at m/z 247.9788 was isolated  
242 and fragmented. Fragmentation spectrum showed intense peak for nitrophenol at m/z 138.0197.

243 In positive mode, peak for Parathion-methyl at m/z 264.0090 could be detected in MP-C and  
244 MP-t<sub>48h</sub>. However, peak of amino-parathion-methyl at m/z 234.0349 was only detected in MP-t  
245 samples, absent in MP-C. Isolation and fragmentation of amino-parathion-methyl in MP-t<sub>48h</sub> did  
246 not yield a *p*-aminophenol fragment; However, fragment with the m/z of 124.9821 representing  
247 *O*-methyl-phosphorothiate could be detected (**Fig. S16**).

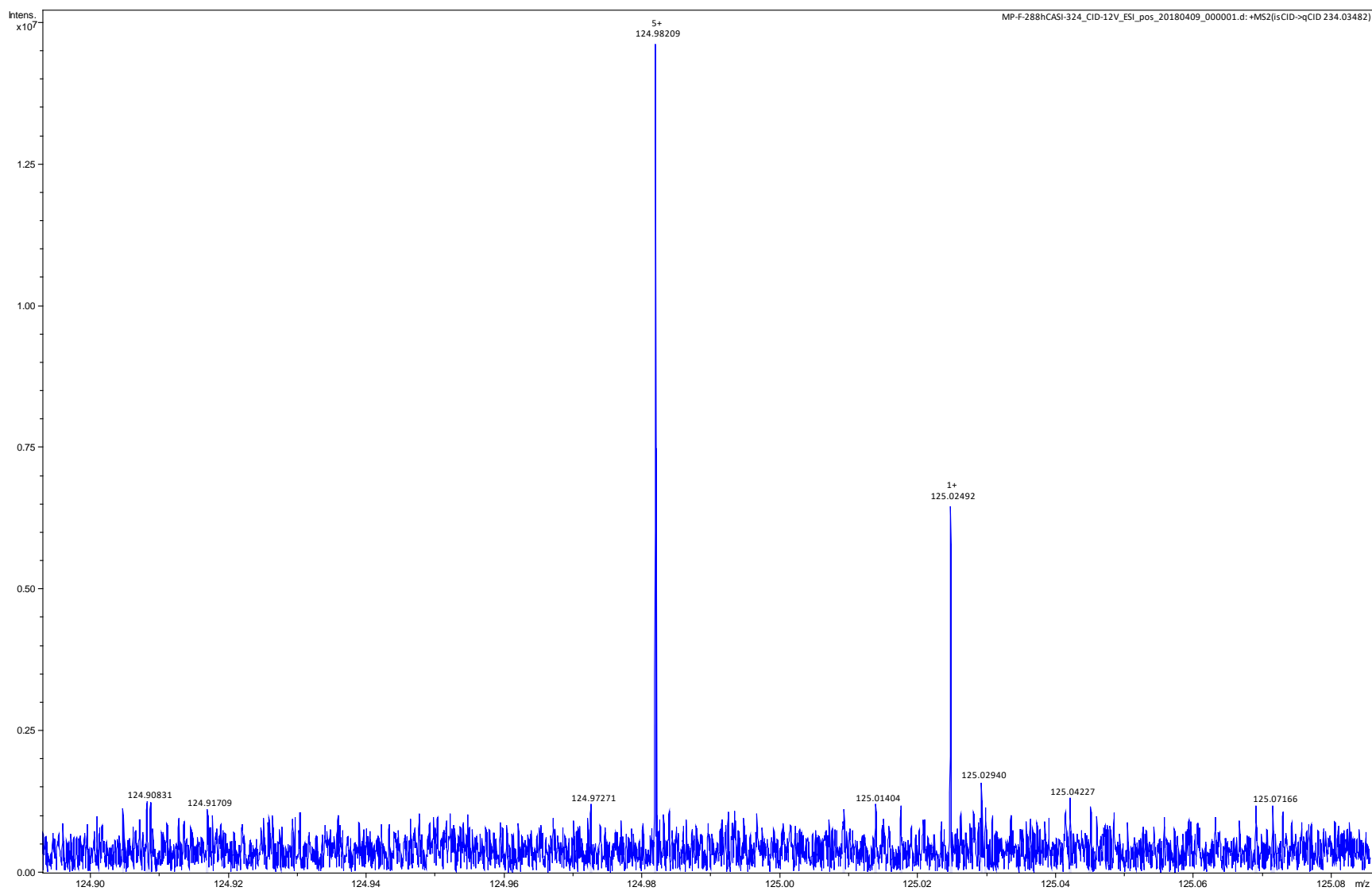
248



249 **Fig S14.** *O*-methyl *O*-(4-nitrophenyl) phosphorothioate with  $m/z$  247.9788 in MP-C.



250 **Fig. S15.** Peak for amino-parathion-methyl at m/z 234.0349 in MP-t<sub>48h</sub>.



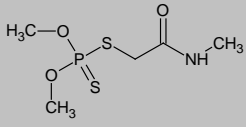
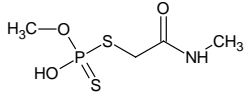
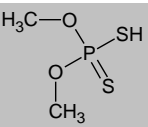
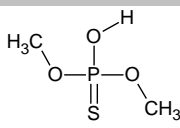
251 **Fig. S16.** Isolation and fragmentation of amino-parathion-methyl at m/z 124.9821.

252 **S5.2.5. Dimethoate (O,O-dimethyl S-[2-(methylamino)-2-oxoethyl] phosphorodithioate)**

253 A sample incubated with biogas slurry was sacrificed after 7h. Metabolites are detected in all

254 samples

255 **Table S6. Proposed metabolites of Dimethoate**

#	Name	Formula	structure	[M+H <sup>+</sup> ] <sup>+</sup>	[M-H <sup>+</sup> ] <sup>-</sup>	m/z detected (intensity)
<b>Parent compound</b>	Dimethoate	C <sub>5</sub> H <sub>12</sub> NO <sub>3</sub> PS <sub>2</sub>		230.0069	227.9923	pos: OP-C: 2.56×10 <sup>9</sup> OP-0: 1.60×10 <sup>10</sup> OP-t: 1.37×10 <sup>10</sup> neg: OP-C: 9.69×10 <sup>9</sup> OP-0: 5.55×10 <sup>9</sup> OP-t: 6.26×10 <sup>9</sup>
<b>1</b>	O-methyl S-[2-(methylamino)-2-oxoethyl] dithiophosphate	C <sub>4</sub> H <sub>10</sub> NO <sub>3</sub> PS <sub>2</sub>		215.9912	213.9767	neg: OP-C: 5.87×10 <sup>11</sup> OP-0: 1.22×10 <sup>11</sup> OP-t: 1.33×10 <sup>11</sup>
<b>2</b>	O,O-dimethyl hydrogen phosphorodithioate	C <sub>2</sub> H <sub>7</sub> O <sub>2</sub> PS <sub>2</sub>		158.9698	156.9552	neg: OP-C: 1.66×10 <sup>10</sup> OP-0: 2.75×10 <sup>9</sup> OP-t: 3.10×10 <sup>9</sup>
<b>3</b>	O,O-dimethyl hydrogen phosphorothioate	C <sub>2</sub> H <sub>7</sub> O <sub>3</sub> PS		142.9926	140.9780	pos: OP-C: n.d. OP-0: 9.27×10 <sup>6</sup> OP-t: 5.82×10 <sup>6</sup>
<b>3*</b> <b>(sodium adduct)</b>				164.9746 [M+Na <sup>+</sup> ] <sup>+</sup>		pos: OP-C: 3.30×10 <sup>7</sup> OP-0: 4.64×10 <sup>7</sup> OP-t: 3.91×10 <sup>7</sup>

256 neg: negative mode; pos: positive mode; n.d.: not detected.

257

258

259 **S5.2.6. Malathion (O,O-dimethyl S-(1,2-dicarbethoxyethyl) phosphorodithioate)**

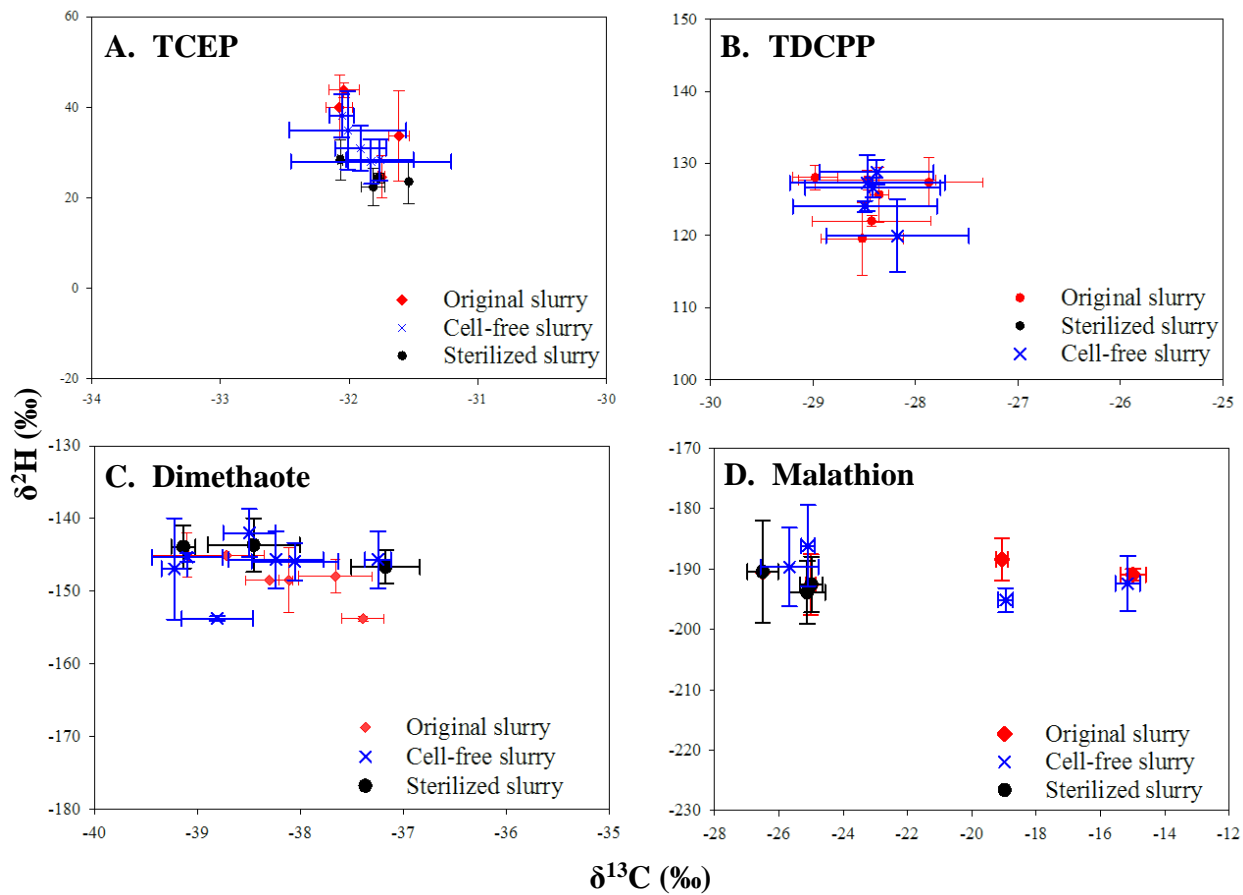
260 Sample incubated with biogas slurry was sacrificed at 13h.

261 **Table S7. Proposed metabolites of Malathion**

#	Name	Formula	structure	[M+H <sup>+</sup> ] <sup>+</sup>	[M-H <sup>+</sup> ] <sup>-</sup>	m/z detected (intensity)	
	Parent compound	Malathion	<chem>C10H19O6PS2</chem> 2		331.0433	329.0288	pos: OP-C: 2.30×10 <sup>9</sup> OP-0: 9.04×10 <sup>9</sup> OP-t: 8.91×10 <sup>9</sup> neg: OP-C: 0.79×10 <sup>9</sup> OP-0: 0.99×10 <sup>9</sup> OP-t: 1.56×10 <sup>9</sup>
1	diethyl 2- {[hydroxy(methoxy)phosphorothioyl]sulfanyl}succinate	<chem>C9H17O6PS2</chem>		317.0277	315.0131	neg: OP-C: 1.26×10 <sup>10</sup> OP-0: 0.27×10 <sup>10</sup> OP-t: 2.29×10 <sup>10</sup>	
1*	(sodium adduct)			339.0096 [M+Na <sup>+</sup> ] <sup>+</sup>		pos: OP-C: 5.91×10 <sup>9</sup> OP-0: 3.6×10 <sup>8</sup> OP-t: 7.5×10 <sup>8</sup>	
2	O,O-dimethyl hydrogen phosphorodithioate	<chem>C2H7O2PS2</chem>		158.9698	156.9552	neg: OP-C: 6.21×10 <sup>10</sup> OP-0: 1.7×10 <sup>9</sup> OP-t: 4.6×10 <sup>9</sup>	
2*	(sodium adduct)			180.9517 [M+Na <sup>+</sup> ] <sup>+</sup>		pos: OP-C: 1.53×10 <sup>7</sup> OP-0: 1.74×10 <sup>7</sup> OP-t: 1.55×10 <sup>7</sup>	
3	O,O-dimethyl hydrogen phosphorothioate	<chem>C2H7O3PS</chem>		142.9926	140.9781	neg: OP-C: 3.73×10 <sup>9</sup> OP-0: 0.42×10 <sup>9</sup> OP-t: 5.50×10 <sup>9</sup>	
3*	(sodium adduct)			164.9746 [M+Na <sup>+</sup> ] <sup>+</sup>		pos: OP-C: 0.64×10 <sup>7</sup> OP-0: 0.75×10 <sup>7</sup> OP-t: 1.02×10 <sup>7</sup>	

262 neg: negative mode; pos: positive mode.

263 **S6. 2D-plot for TCEP, TDCPP, Dimethoate and Malathion**



264

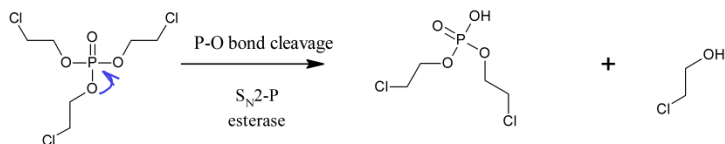
265 **Fig. S17.** 2D-CSIA plots of enzymatic hydrolysis in slurry of biogas reactor and abiotic

266 hydrolysis of TCEP, TDCPP, Dimethoate and Malathion.

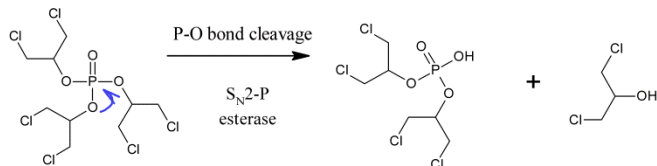
267 **Scheme S2.** Proposed transformation pathways of TCEP, TDCPP, Dimethoate and Malathion in

268 biogas slurry

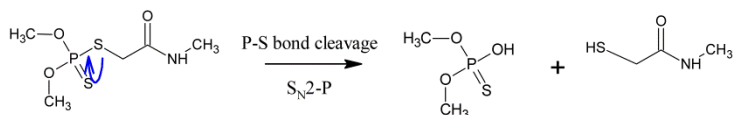
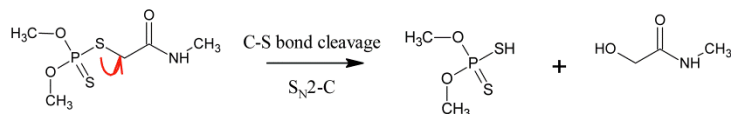
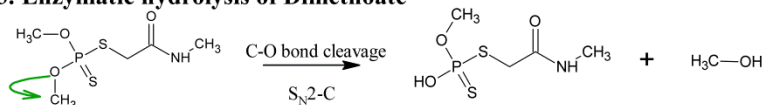
### 1. Enzymatic hydrolysis of TCEP



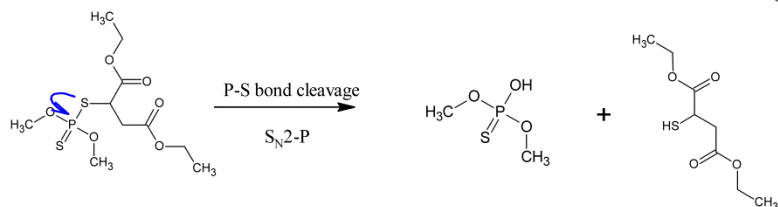
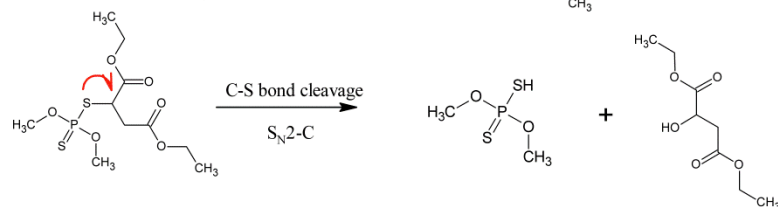
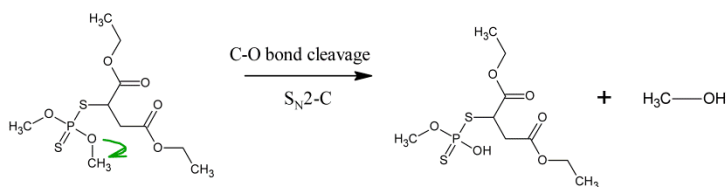
### 2. Enzymatic hydrolysis of TDCPP



### 3. Enzymatic hydrolysis of Dimethoate



### 4. Enzymatic hydrolysis of Malathion



269

270

271 **S7. Methylation as subsequent reaction**

272 Methylation of the metabolites was found in Parathion-methyl and Dimethoate experiments. For  
273 instance, the metabolite after the P-O bond cleavage was methylated to *O,O,O*-  
274 trimethylthiophosphate in Parathion-methyl set and *O,O,S*-trimethyl phosphorodithioate was  
275 formed with methylation after S-C bond cleavage in Dimethoate. It is assumed that methylation  
276 is associated with methyltransferases in the AD system. However, this subsequent reaction did  
277 not affect the isotope fractionation of the parent compound.

278 Methylation of the metabolites was found in Parathion-methyl and Dimethoate experiments. For  
279 instance, *O,O,O*-trimethylthiophosphate was generated after the P-O bond cleavage in Parathion-  
280 methyl set and phosphorodithioic acid, *O,O,S*-trimethylester was formed with methylation after  
281 S-C bond cleavage in Dimethoate. It is assumed that methylation is associated with  
282 methyltransferases in the AD system.

283 Among the methyltransferases, non- *S*-Adenosyl methionine (SAM) dependent  
284 methyltransferases using the cofactor vitamin B<sub>12</sub> and tetrahydrofolate (Ragsdale, 2008), and  
285 natural product methyltransferases (NPMTs), which mostly depended on SAM (Liscombe et al.,  
286 2012), are putative enzymes for the methyl group transfers in anoxic condition (Jäger and Croft,  
287 2018). The typical non-SAM dependent methyltransferases involved in methanogenesis of AD  
288 use tetrahydromethanopterin and coenzyme M as methyl acceptors for methane conversion  
289 (Thauer, 1998). NPMTs contain a diverse group of enzymes which take naturally-produced small  
290 molecules as acceptors, adding methyl group to S, N, O, or C atom for formation of metabolites.  
291 Thus, it is inferred that the methylation of OPs in AD process is attributed to NPMTs.

292

293 **References**

294 Jäger, C.M., Croft, A.K., 2018. Anaerobic radical enzymes for biotechnology. *ChemBioEng Rev.*  
295 5, 143–162.

296 Liscombe, D.K., Louie, G. V., Noel, J.P., 2012. Architectures, mechanisms and molecular  
297 evolution of natural product methyltransferases. *Nat. Prod. Rep.* 29, 1238–1250.

298 Ragsdale, S.W., 2008. Catalysis of methyl group transfers involving tetrahydrofolate and B12.  
299 *Vitam. Horm.* 79, 293–324.

300 Thauer, R.K., 1998. Biochemistry of methanogenesis: a tribute to Marjory Stephenson.  
301 *Microbiology* 144, 2377–2406.

302 Wu, L., Chládková, B., Lechtenfeld, O.J., Lian, S., Schindelka, J., Herrmann, H., Richnow, H.H.,  
303 2018. Characterizing chemical transformation of organophosphorus compounds by  $^{13}\text{C}$  and  
304  $^2\text{H}$  stable isotope analysis. *Sci. Total Environ.* 615, 20–28.

305 Wu, L., Yao, J., Trebse, P., Zhang, N., Richnow, H.H., 2014. Compound specific isotope  
306 analysis of organophosphorus pesticides. *Chemosphere* 111, 458–463.

307